The Astronomical Journal, 130:896–922, 2005 September

A COMPLETE SAMPLE OF MEGAPARSEC-SIZED DOUBLE RADIO SOURCES FROM THE SYDNEY UNIVERSITY MOLONGLO SKY SURVEY

L. Saripalli,[1] R. W. Hunstead,[2] R. Subrahmanyan,[1] and E. Boyce[2,3]

Received 2005 March 24; accepted 2005 May 16

ABSTRACT

We present a complete sample of megaparsec-sized double radio sources compiled from the Sydney University Molonglo Sky Survey. Almost complete redshift information has been obtained for the sample. The sample has the following defining criteria: Galactic latitude $|b| > 12.^{\circ}5$, declination $\delta < -50^{\circ}$, and angular size $>5'$. All the sources have a projected linear size larger than 0.7 Mpc (assuming $H_0 = 71$ km s^{-1} Mpc^{-1}). The sample is chosen from a region of the sky covering 2100 deg^2. In this paper we present 843 MHz radio images of the extended radio morphologies made using the Molonglo Observatory Synthesis Telescope, higher resolution radio observations of any compact radio structures using the Australia Telescope Compact Array, and low-resolution optical spectra of the host galaxies from the 2.3 m Australian National University telescope at Siding Spring Observatory. The sample presented here is the first in the southern hemisphere and significantly enhances the database of known giant radio sources. The giant radio sources with linear size exceeding 0.7 Mpc have an abundance of (215 Mpc)$^{-3}$ at the sensitivity of the survey. In the low-redshift universe, the survey may be suggesting the possibility that giant radio sources with relict lobes are more numerous than giant sources in which beams from the center currently energize the lobes.

Key words: galaxies: active — galaxies: distances and redshifts — radio continuum: galaxies — surveys

1. INTRODUCTION

Double radio sources of large linear size—the giant radio sources—form a valuable resource for understanding the radio galaxy phenomenon and probing the intergalactic medium (Subrahmanyan & Saripalli 1993). Their large sizes raise several interesting questions concerning not only their formation but also issues related to the long lifetime of their nuclear beam activity and jet stability. The long timescales involved also imply that the radio structures of these giant radio sources might show evidence of changes in nuclear activity that might be linked to recent merger events or other triggers of central engine activity. Recent discoveries of radio sources with inner double structures embedded within more relaxed outer diffuse lobes (Subrahmanyan et al. 1996; Schoenmakers et al. 2000a; Saripalli et al. 2002, 2003) have drawn attention to the phenomenon of restarting in beams. Investigations into these issues clearly benefit from having large numbers of giant radio sources and, importantly, samples with uniform selection criteria.

The number of known giant radio sources has grown largely from serendipitous discoveries over the years. However, there have been several attempts in the last decade to make directed searches for these large objects. Low-frequency radio surveys with high surface brightness sensitivity are especially suited for the purpose of detecting giant radio sources. Cotter et al. (1996) presented a sample of giant radio sources selected from the Cambridge Low-Frequency Synthesis Telescope 7C survey. The Westerbork Northern Sky Survey (WENSS; Rengelink et al. 1997) was used by Schoenmakers et al. (2001) to compile a complete flux density–limited sample of giant radio sources. Lara et al. (2001) and also Machalski et al. (2001) compiled samples of large angular size sources using the NRAO VLA Sky Survey (NVSS; Condon et al. 1998) and the Faint Images of the Radio Sky at Twenty cm (FIRST; Becker et al. 1995) survey and worked toward identifying giant radio sources in these surveys. In this paper we describe a similar effort that has resulted in the formation of a complete sample of giant radio sources in the southern hemisphere based on the Sydney University Molonglo Sky Survey (SUMSS).

The SUMSS has been described in detail elsewhere (Bock et al. 1999; Mauch et al. 2003). The 843 MHz SUMSS was started in 1997 and uses the upgraded Molonglo Observatory Synthesis Telescope (MOST) as the survey instrument. With a synthesized beam of FWHM $= 45 \csc|\delta| \times 45$ arcsec^2 at a position angle of 0°, an rms noise level of $\sim$1 mJy beam^{-1}, and excellent spatial frequency coverage, the survey is one of the most sensitive to date for extended sources. The sample presented in this paper is from the region observed up to the end of 2000 February and covers 2100 deg^2. In § 2 we describe the methodology adopted for initially selecting candidate giant radio sources in this sky region. Subsequently, we carried out high-resolution Australia Telescope Compact Array (ATCA) radio observations for detecting radio cores in these candidates, and this is reported in § 3. Spectroscopy of the optical identifications made at the locations of the radio cores is presented in § 4. The resulting giant radio source sample is presented, along with notes on individual sources in § 5. In § 6 we discuss the sample properties. The candidates that were rejected while forming the complete sample are discussed in Appendix A.

Giant radio sources are usually defined in the literature to be double radio sources with projected linear size greater than 1 Mpc; this limit was based on a Hubble constant of $H_0 = 50$ km s^{-1} Mpc^{-1}. We adopt a flat cosmology with Hubble constant $H_0 = 71$ km s^{-1} Mpc^{-1} and matter density parameter $\Omega_m = 0.27$. Double radio sources with linear size exceeding 0.7 h_{71}^{-1} Mpc are large enough to be atypical, and most of the extended radio structure would lie well outside of gas associated

[1] CSIRO Australia Telescope National Facility, Locked Bag 194, Narrabri, NSW 2390, Australia; lakshmi.saripalli@csiro.au, ravi.subrahmanyan@csiro.au.

[2] School of Physics, University of Sydney, Sydney, NSW 2006, Australia; rwh@physics.usyd.edu.au.

[3] Kavli Institute, Massachusetts Institute of Technology, 77 Massachusetts Avenue, Cambridge, MA 02139; eboyce@mit.edu.

with the host galaxy; however, there is no reason for adopting a definitive linear size cutoff apart from having well-defined sample selection criteria. For consistency with previous work, we have chosen to include in our final sample all radio galaxies with linear sizes larger than 0.7 Mpc for our adopted H_0.

2. THE SUMSS GIANT RADIO SOURCE CANDIDATES

Boyce (2000) examined the sky area covered by SUMSS prior to 2000 February for candidate giant radio sources; at that time SUMSS was 26% complete. Boyce also limited the search to declinations $\delta < -50^\circ$ and Galactic latitudes $|b| > 12.^\circ5$. A total of 2100 deg^2 of sky area was examined by eye. At the low frequency of 843 MHz and the low resolution of $\approx 45''$, the lobes rather than cores or hot spots of extragalactic double radio sources dominate the images. A search was made for single connected structures that have a large angular size, close pairs of extended radio components—double sources that appeared to be extended along the line joining the two components—and any triple sources. The angular extent was estimated to be the separation between the peaks of the outermost components, and only sources with angular size exceeding $5'$ were deemed to be candidate giant radio sources. A total of 35 candidates were selected as potential giant radio sources.

In this paper we adopt a nomenclature for sources that identifies the survey and their giant nature. The giant radio sources that satisfied the selection criteria are given the prefix SGRS (SUMSS giant radio source), and the remainder of the candidate list are given the prefix SGRSC (SUMSS giant radio source candidate). It may be noted that some of the candidates in Appendix A have linear sizes exceeding 0.7 Mpc and are giant radio sources, some are double radio sources with smaller linear size, and some are composed of unrelated components.

Twelve extended double radio sources (SGRSC J0020−7321, J0129−6433, J0200−6007, J0534−8203, J0551−5655, J0603−5429, J0622−5938, J1959−6402, J2150−6210, J2222−5617, J2228−5600, and J2253−5813) were detected in the search area with angular sizes, measured from the SUMSS images, that were close to the limit of $5'$ but below the angular size cutoff. We included them in follow-up high-resolution radio imaging to test whether there were any giant radio sources among them. As discussed below, the follow-up observations revealed that some of these double/triple components were unrelated sources and some had linear sizes smaller than 0.7 Mpc.

For the two sources SGRS J0143−5431 and SGRS J0326−7730, the emission peak in one of the lobes was displaced well away from the edge, unlike the other candidates. For these two sources we identified components representing the extended emission with a Gaussian fit to a slice along the lobe. The angular extents for the sources were estimated using these identified components.

The selection criteria included a declination limit so that the SUMSS radio images and the follow-up with the east-west ATCA had synthesized beams that were not too elongated. Low Galactic latitudes were avoided to facilitate optical identifications. The lower limit of $5'$ on the angular size was chosen to include essentially all powerful edge-brightened double radio sources in the nearby universe with total linear size larger than 0.7 Mpc and to ensure that the candidate list did not overwhelm our resources for radio/optical follow-up; this criterion was the same as that adopted by Schoenmakers et al. (2001). The angular size cutoff, together with the sensitivity limit of the survey, potentially discriminates against edge-darkened (Fanaroff-Riley type I [FR I]) double radio sources; even if the largest angular size in edge-darkened sources exceeds $5'$, it is possible that the separation between the peaks in their lobes is less than this cutoff, and such sources might be missed. Effectively, this criterion implies almost a factor of 2 larger linear size cutoff for FR I sources in any redshift bin.

For the adopted cosmology, the selection criteria imply that our giant radio source sample will be complete for redshifts $z \leq 0.13$: all edge-brightened giant sources with linear size exceeding 0.7 Mpc are detectable within the corresponding 3.5×10^7 Mpc^3 comoving volume. At redshifts exceeding 0.13, only sources with progressively larger linear size would be selected. Powerful double radio sources with edge-brightened structure have radio power exceeding about 1.3×10^{25} W Hz^{-1} at 843 MHz, corresponding to the FR I/FR II break power (Owen & Ledlow 1994). In our adopted cosmology, such sources would be detectable in SUMSS with flux density exceeding 0.3 Jy if they were at redshifts $z \leq 0.13$.

3. ATCA RADIO OBSERVATIONS OF THE CANDIDATE LIST

We observed the candidate list of 35 large angular size sources at higher resolution using ATCA for the purpose of detecting compact radio cores that could guide the optical identification process. The ATCA observations were also aimed at examining the compact structures in the individual components as a means of identifying cases in which the close components were independent sources or chance alignments.

All 35 sources were observed in 24 hr observing sessions using the 6A and 6D east-west configurations of ATCA during 2001 November–December (Table 1). The multichannel continuum observations were made in the 20 cm band using a pair of 128 MHz bands centered at 1344 and 1440 MHz. Every source was observed at four or five widely spaced hour angles, each of about 6 minutes duration. The data were reduced in MIRIAD using an automated script with parameters optimized for imaging point sources. Multifrequency synthesis was used to make a combined image using the data from the two adjacent frequencies; the images had beam FWHMs in the range $5''-10''$. The rms noise in the deconvolved images varied between 0.2 and 1.0 mJy beam^{-1}; the images were dynamic range–limited owing to the sparse visibility coverage.

Cores were undetected or could not be unambiguously identified in five cases (SGRSC J0020−7321, SGRSC J0622−5938, SGRS J0326−7730, SGRS J0810−6800, and SGRS J1259−7737). We reobserved these five sources in the 6 cm band using ATCA in the 6A configuration during 2002 November (see Table 2). These multichannel continuum observations were made using a pair of 128 MHz bands centered at 4800 and 5952 MHz. Each target was observed for a total of 4 hr, with the total time distributed over hour angle as before. Bandwidth synthesis was used to image the visibility data in MIRIAD; the images had beam FWHMs in the range $2''-3''$. The rms noise in the resulting images was about 0.03 mJy beam^{-1}. Excepting SGRSC J0622− 5938, the observations showed compact cores between the diffuse radio components in all the doubtful cases.

In sources of large angular size, the region between the lobes where one might expect to find a radio core coincident with an optical counterpart is large, and therefore, there might be ambiguities in the identification of the host. In some cases, supporting evidence such as connected lobe emission or jetlike features might provide confirmation for the identification. Examining the high-resolution ATCA images that we used for detecting the radio cores of the giant radio galaxy candidates, we find that there is on the average about 1 compact radio source coincident with an optical galaxy in regions of about 140 arcmin^2 (avoiding

TABLE 1
JOURNAL OF ATCA OBSERVATIONS AT 1.4 GHz

Name	Array	Date	Time (minutes)
SGRSC J0020−7321.....	6D	2001 Nov 26	28
	6A	2001 Dec 14	24
SGRS J0047−8307.....	6D	2001 Nov 26	28
	6A	2001 Dec 14	24
SGRSC J0129−6433.....	6D	2001 Nov 25	24
	6A	2001 Dec 14	24
SGRS J0143−5431.....	6D	2001 Nov 26	21
	6A	2001 Dec 14	24
SGRSC J0152−8020.....	6D	2001 Nov 25	28
	6A	2001 Dec 14	24
SGRSC J0200−6007.....	6D	2001 Nov 25	33
	6A	2001 Dec 14	24
SGRS J0237−6429.....	6D	2001 Nov 25	28
	6A	2001 Dec 14	24
SGRS J0326−7730.....	6D	2001 Nov 25	35
	6A	2001 Dec 14	24
SGRS J0331−7710.....	6D	2001 Nov 25	33
	6A	2001 Dec 14	24
SGRS J0400−8456.....	6D	2001 Nov 25	28
	6A	2001 Dec 14	24
	1.5A	2004 Mar 21	375
	1.5A	2004 Mar 30	310
SGRSC J0414−6933.....	6D	2001 Nov 25	35
	6A	2001 Dec 14	24
	1.5A	2004 Mar 30	260
SGRS J0515−8100.....	6D	2001 Nov 25	35
	6A	2001 Dec 14	24
SGRSC J0534−8203.....	6D	2001 Nov 25	35
	6A	2001 Dec 14	24
SGRSC J0551−5655.....	6D	2001 Nov 25	35
	6A	2001 Dec 14	24
SGRSC J0603−5429.....	6D	2001 Nov 25	28
	6A	2001 Dec 14	24
SGRSC J0622−5938.....	6D	2001 Nov 25	28
	6A	2001 Dec 14	24
SGRS J0631−5405.....	6D	2001 Nov 25	28
	6A	2001 Dec 14	24
SGRSC J0745−7732.....	6D	2001 Nov 25	38
	6A	2001 Dec 14	36
SGRS J0746−5702.....	6D	2001 Nov 25	35
	6A	2001 Dec 14	36
SGRS J0810−6800.....	6D	2001 Nov 25	35
	6A	2001 Dec 14	30
SGRS J0843−7007.....	6D	2001 Nov 25	35
	6A	2001 Dec 14	30
SGRS J1259−7737.....	6D	2001 Nov 25	35
	6A	2001 Dec 14	36
SGRS J1336−8019.....	6D	2001 Nov 25	35
	6A	2001 Dec 14	36
SGRS J1728−7237.....	6D	2001 Nov 25	42
	6A	2001 Dec 14	36
SGRS J1911−7048.....	6D	2001 Nov 25	35
	6A	2001 Dec 14	30
SGRS J1919−7959.....	6D	2001 Nov 26	28
	6A	2001 Dec 14	24
SGRSC J1920−7753.....	6D	2001 Nov 26	21
	6A	2001 Dec 14	24
	1.5A	2004 Apr 4	312
SGRS J1946−8222.....	6D	2001 Nov 26	21
	6A	2001 Dec 14	24
SGRSC J1959−6402.....	6D	2001 Nov 26	21
	6A	2001 Dec 14	25
SGRSC J2150−6210.....	6D	2001 Nov 26	28
	6A	2001 Dec 14	24
SGRS J2159−7219.....	6D	2001 Nov 26	28
	6A	2001 Dec 14	24
SGRSC J2222−5617.....	6D	2001 Nov 26	21
	6A	2001 Dec 14	24
SGRSC J2228−5600.....	6D	2001 Nov 26	21
	6A	2001 Dec 14	24
SGRSC J2253−5813.....	6D	2001 Nov 26	21
	6A	2001 Dec 14	24
SGRSC J2336−8151.....	6D	2001 Nov 26	28
	6A	2001 Dec 14	24

the regions close to the giant radio sources). On the average, the sky area that we searched for optical counterparts of individual giant radio source candidates is about 5 arcmin^2. We infer that the probability of the occurrence of a random compact object in the area where we look for optical identifications is 0.04 and that ambiguities might be expected in only 4% of the cases.

In five sources (SGRSC J0200−6007, J0603−5429, J1959−6402, J2150−6210, and J2253−5813), the angular separation between compact components that were detected at the ends of the extended SUMSS components was less than 5′, and therefore, these sources were excluded from further consideration for our giant radio source sample. In SGRSC J0020−7321 and SGRSC J0129−6433 the ATCA observations revealed a compact component in only one lobe, and in SGRSC J2228−5600 no hot spots were seen; the ends of these sources as seen on SUMSS images were separated by $\lesssim$5′, and they were not included in the complete sample. However, they were retained for the optical spectroscopy.

The connectedness between the close components in SGRS J0400−8456, SGRSC J0414−6933, and SGRSC J1920−7753 was not established in the SUMSS images; therefore, we made somewhat higher resolution 20 cm band ATCA observations of these sources in 1.5 km configurations. The southwestern component of SGRSC J1920−7753 was observed to have a triple structure and is probably an independent radio source. The northernmost component of SGRSC J0414−6933 appeared to be a separate unresolved source, and the remainder a triple of angular size less than 5′. Therefore, these two sources are rejected by our selection criteria. Two other sources (SGRSC J0622−5938 and J0745−7732) were rejected because an examination of their SUMSS extended structure together with the ATCA compact components suggested that these source structures are peculiar and are very unlike our expectations for double radio sources. The details of these observations are given below in § 5 and in Appendix A as part of the notes on individual sources.

TABLE 2
JOURNAL OF ATCA OBSERVATIONS AT 4.8 GHz

Name	Array	Date	Time (minutes)
SGRSC J0020−7321.....	6A	2002 Nov 22	227
SGRS J0326−7730.....	6A	2002 Nov 22	268
SGRSC J0622−5938.....	6A	2002 Nov 22	152
SGRS J0810−6800.....	6A	2002 Nov 22	160
	6C	2004 May 15	160
SGRS J1259−7737.....	6A	2002 Nov 22	170

Composite images made by overlaying ATCA radio contours on SuperCOSMOS Sky Survey (SSS) gray scales were examined for any optical counterparts. In some cases, the optical images showed galaxies coincident with compact radio components located within each of the close pair of extended radio sources. These were deemed to be separate radio sources created by the separate optical identifications and not related double structures created by twin beams from a single active galactic nucleus. There were four such candidates (SGRSC J0152−8020, J0534−8203, J0551−5655, and J2222−5617) that were rejected for this reason.

There were, in all, 22 giant radio source candidates that satisfied the criteria of angular size, declination, and latitude.

4. OPTICAL SPECTROSCOPY OF THE HOST GALAXIES

The redshifts of 6 of the 22 giant radio source candidates had been measured previously (SGRSC J0020−7321, SGRSC J2336−8151, SGRS J0143−5431, SGRS J1919−7959, and SGRS J2159−7219: Boyce 2000; SGRS J0515−8100: R. Subrahmanyan et al. 2005, in preparation). The spectra in Boyce (2000) were obtained in service mode at the 3.9 m Anglo-Australian Telescope. The remaining 16 were observed in multiple sessions using the Dual Beam Spectrograph (DBS) on the Australian National University (ANU) 2.3 m telescope (Rodgers et al. 1988) to obtain optical spectra for measuring redshifts. A journal of the optical spectroscopy is presented in Tables 3 and 4.

We were initially allocated a total of seven nights of dark time. These were in two separate observing runs in 2002 August (four nights) and 2002 November (three nights), and 14 objects were observed in these sessions (Table 3). Only the last night in the August session and the later two nights in the November session were without cloud for most of the night; these had an average seeing of $\approx 1\farcs7$. The other nights were mostly lost because of cloud.

Three of the objects were too faint to give reliable redshifts. In addition, the identifications of two other sources were revised on the basis of ATCA observations that were scheduled following the optical spectroscopy. We reobserved three of these candidates—SGRS J0810−6800 (new ID), J1911−7048, and J1946−8222—along with SGRS J1259−7737, which had not been observed in the earlier sessions, on two additional nights in 2004 April. These nights were clear, with an average seeing of $1\farcs5$. The two other sources—SGRS J0237−6429 and SGRS J0326−7730 (new ID)—were observed in a separate run in 2004 September. These later observations are listed in Table 4.

TABLE 3

Journal of Optical Spectroscopy Observations in 2002

Name	Magnitude (b_J)	Date	Exposure (s)
SGRS J0047−8307	20.2	2002 Aug 4	2000
		2002 Nov 5	2000
SGRSC J0129−6433	18.5	2002 Aug 2	2000
SGRS J0237−6429	20.9	2002 Aug 4	2000
		2002 Nov 3	2000
SGRS J0331−7710	18.2	2002 Aug 4	2000
		2002 Nov 4	2000
SGRS J0400−8456	16.9	2002 Nov 4	2000
		2002 Nov 5	2000
SGRS J0631−5405	16.9	2002 Nov 4	2000
SGRS J0746−5702	18	2002 Nov 4	2000
SGRS J0810−6800		2002 Nov 5	2000
SGRS J0843−7007	17.7	2002 Nov 5	2000
SGRS J1336−8019	16.7	2002 Aug 3	2000
SGRS J1728−7237	21	2002 Aug 1	2000
		2002 Aug 2	2000
SGRS J1911−7048	19.4	2002 Nov 5	2000
SGRS J1946−8222	22.3	2002 Aug 4	2000
SGRSC J2228−5600	17.5	2002 Aug 2	2000

TABLE 4

Journal of Optical Spectroscopy Observations in 2004

Name	Magnitude (b_J)	Date	Exposure (s)
SGRS J0237−6429	20.9	2004 Sep 13	2×1500
SGRS J0326−7730	20.7	2004 Sep 13	2×1500
SGRS J0810−6800	16.3	2004 Apr 15	4×2000
SGRS J1259−7737	22.4	2004 Apr 15	5×2000
SGRS J1911−7048	19.4	2004 Apr 14	3×2000
SGRS J1946−8222	22.3	2004 Apr 14	4×2000

A low-resolution grating, 158R lines mm^{-1}, was used, giving a wavelength coverage of 3600–10900 Å with a spectral resolution of 8 Å ($\sim$2 pixels). The red arm of the DBS was used for the observations listed in Table 3, whereas the blue arm was used for the observations listed in Table 4. Most objects were observed in a single 2000 s exposure; however, fainter objects required longer integration times. To calibrate for atmospheric absorption, a smooth-spectrum star was also observed at roughly the same zenith angle as the target observations. In the 2002 observing runs each target and smooth-spectrum standard frame was sandwiched between two short exposures of a Ne-Ar arc for wavelength calibration; a Cu-Ar arc was used in the later runs. A slit width of $2''$ was used for the target observations, as well as the arc exposures.

The standard IRAF reduction package was used for the analysis. The raw two-dimensional spectra were corrected for CCD bias, after which they were flat-fielded using averaged dome and sky flats. In extracting the one-dimensional spectra of the targets, the sky background was averaged over nearby rows on either side of the target trace to minimize effects due to curvature in the spatial axis. Cosmic rays were removed by setting the flux ratio parameter for a given flux threshold using the COSMICRAYS procedure; the flux ratio versus threshold plot of the CCD frame was examined to set the values. This method worked well enough up to a certain flux ratio, but beyond that it was nearly impossible to reduce the value further without also affecting the target spectrum adversely. Objects observed in the sessions listed in Table 4 had multiple exposure frames, and, after calibration, these were combined using SCOMBINE; the resulting spectra were relatively free of artifacts. The one-dimensional spectra were divided by the normalized fit to the continuum of a smooth-spectrum star to remove atmospheric absorption.

We used the IRAF task RVIDLINES to determine the redshifts. We checked for broad consistency between the redshift and the apparent magnitude of the target. Several objects were independently analyzed by two of us, using different software packages, and we obtained identical results: this gives us confidence in the redshift estimates.

The redshifts were used to derive the linear sizes of the 22 candidates. Four sources (SGRSC J0020−7321, J0129−6433, J2228−5600, and J2336−8151) had linear size <0.7 Mpc and were excluded from the giant radio source sample on this basis. We were unable to obtain a reliable spectrum for SGRS J1259−7737 because of the faintness of the optical host; assuming that the faintness implies a high redshift, we have chosen to retain

this source in our giant radio source sample (see the notes on this source in § 5.1).

5. RESULTS

Table 5 presents the final sample of 18 radio sources satisfying the criteria $|b| > 12.^{\circ}5$, $\delta < -50^{\circ}$, angular size >5′, and linear size larger than 0.7 Mpc; the table lists some observed properties of the sources. In order to estimate the angular sizes of the giant radio sources, we measured the peak-to-peak separation using the higher resolution ATCA images in those cases in which hot spots were detected at both ends and used the SUMSS 843 MHz maps for the remaining sources. Table 6 lists the positions and flux densities of the radio cores in these 18 giant radio sources. The radio sources in the initial list of candidates that were deemed not to be giant radio sources on the basis of the radio-optical follow-up observations are listed separately in Appendix A, along with their observational data.

The composite radio images of all 18 giant radio sources are given in Figures 1–18; contours of the higher resolution ATCA images are shown using thin lines, and the low-resolution SUMSS images are shown using thick contours; these are shown overlaid on gray-scale representations of SSS optical fields.

The optical spectra of the host galaxies of the giant radio sources are shown in Figure 19. The spectra are not flux calibrated. The reduced spectra often have spurious features as a result of errors in sky subtraction and cosmic rays, and we have identified some of these in Figure 19. In Table 7 we list the lines identified in the different objects and give the estimated redshifts derived from fits to these lines. Redshifts are based on air wavelengths and have not been corrected to the Sun. In Table 8 we list some source properties derived from the observations, namely, linear sizes, core powers, the integrated source powers, and host absolute magnitudes.

TABLE 5

Observed Properties of the Sample of 18 SUMSS Giant Radio Sources

Name	Redshift	Angular Size (arcmin)	Radio Structure	$S843$[a] (mJy)
SGRS J0047−8307.....	0.2591	5.6	FR II	543
SGRS J0143−5431.....	0.1791	5.5	FR II	217
SGRS J0237−6429.....	0.364:	6.6	FR II	145
SGRS J0326−7730.....	0.2771	5.3	FR II	357
SGRS J0331−7710.....	0.1456	17.7	FR II	687
SGRS J0400−8456.....	0.1037	6.3	FR I	175
SGRS J0515−8100.....	0.1050	7.5	FR I/FR II	264
SGRS J0631−5405.....	0.2036	5.2	FR II	694
SGRS J0746−5702.....	0.1300	5.5	FR I	194
SGRS J0810−6800.....	0.2311	6.5	FR II	271
SGRS J0843−7007.....	0.1381	5.6	FR I	203
SGRS J1259−7737.....	>0.3[b]	5.7	FR II	439
SGRS J1336−8019.....	0.2478	10.1	FR II	483
SGRS J1728−7237.....	0.4735	6.2	FR II	214
SGRS J1911−7048.....	0.2152	6.0	FR II	238
SGRS J1919−7959.....	0.3462	6.0	FR II	1262
SGRS J1946−8222.....	0.333:	7.4	FR II	219
SGRS J2159−7219.....	0.0974	9.2	FR II	142

Note.—Colons denote uncertain values.

[a] Total flux density at 843 MHz.

[b] The redshift lower limit is obtained using $K = 16.2 \pm 0.2$ mag. See § 5.1.12.

5.1. *Notes on Individual Sources*

5.1.1. *SGRS J0047−8307 (Fig. 1)*

In the SUMSS 843 MHz image the source is seen as a triple; there are noticeable gaps in the radio emission between the lobes and the core. The lobe with the smaller separation from the core is also the brighter of the two lobes. The ATCA image shows two compact components in the northwestern lobe; however, in the southern lobe there is only a weak component close to the peak of the extended emission. The extension seen in the southeastern lobe at 843 MHz toward the northwest might be confused with emission associated with a relatively bright $b_J = 17.8$ elliptical galaxy that is host to a compact $S_{1.4} = 6.4$ mJy source. The host galaxy, which is coincident with the radio core, has a close neighbor 5″ to the south and another 12″ to the west. The optical spectrum has a low signal-to-noise ratio.

5.1.2. *SGRS J0143−5431 (Fig. 2)*

The SUMSS 843 MHz image shows a relaxed morphology for the two lobes, and the higher resolution 1.4 GHz ATCA image shows no compact features associated with the lobes. The ATCA image (Fig. 2*b*) shows a radio core and, interestingly, also shows two compact features on either side of the core and along the source axis; this triple structure at the core, together with the relaxed outer lobes, suggests the possibility that SGRS J0143−5431 might be a case in which an inner double has been created by a restarting of the beams from the central engine. The host galaxy has a few, relatively faint neighbors within 15″ radius and a bright galaxy 30″ to the southeast. The close faint neighbor 5″ to the west is a blue object, and the galaxy 12″ to the north is a spiral. The optical spectrum of the host galaxy was obtained by Boyce (2000).

5.1.3. *SGRS J0237−6429 (Fig. 3)*

The SUMSS image shows two lobes, with surface brightness decreasing toward the center and prominent gaps in the emission between the core and the two lobes. The ATCA image shows a weak core and compact features at the ends of both lobes. The closer lobe is also the brighter of the two lobes. The host galaxy does not have any close neighbors. The optical spectrum is very noisy, and the redshift is uncertain.

5.1.4. *SGRS J0326−7730 (Fig. 4)*

This source has an unusual structure. The SUMSS image shows two extended components, of which the southeastern is significantly stronger. The higher resolution 1.4 GHz ATCA image reveals a bright elongated structure in this southeastern lobe. Although edge-brightened, there is no compact unresolved feature toward the outer end of this lobe. The ATCA image also shows a compact component at the peak of the northwestern lobe. The 4.8 GHz ATCA image (Fig. 4*b*) shows a weak core coincident with a faint galaxy that is located within the SUMSS contours of the stronger lobe and close to the line joining the compact features in the two lobes. The host galaxy has several faint galaxies in its neighborhood.

5.1.5. *SGRS J0331−7710 (Fig. 5)*

This radio source has the largest linear size in the sample and is extremely asymmetric in lobe separation, as well as lobe brightness and flux density. Both lobes are highly elongated with high axial ratios, and both elongated lobes are collinear. The two lobes are edge brightened; however, the contrast in surface brightness along the lobe axes is relatively weak in this source. In the ATCA image the two lobes are completely resolved, and a weak core is detected at the inner end of the northern lobe (Fig. 5*b*); there is a significant emission gap of almost 600 kpc between the core and the southern lobe. The host galaxy is fairly isolated except for a

TABLE 6

Results of ATCA Observations of the Giant Radio Source Sample

Name	Other Names	Associated SUMSS Sources	Core Position (J2000.0)		Core Flux Density (mJy)	
			R.A.	Decl.	1.4 GHz	4.8 GHz
SGRS J0047−8307.....	PKS B0046−833	J004756−830816	00 47 55.5	−83 08 12.5	8.3	
	PMN J0047−8307	J004704−830722				
	MRC 0046−833	J004931−830914				
SGRS J0143−5431.....		J014344−543140	01 43 43.2	−54 31 39.0	1.7	
		J014353−543249				
		J014335−542919				
SGRS J0237−6429.....	PMN J0237−6428	J023655−642751	02 37 09.9	−64 30 02.2	2.0	
		J023728−643246				
SGRS J0326−7730.....	PMN J0326−7730	J032514−772928	03 26 01.3	−77 30 16.9	...	0.46
		J032506−772809				
		J032618−773039				
SGRS J0331−7710.....	PKS B0333−773	J033133−771133	03 31 39.8	−77 13 19.3	1.3	
	PMN J0331−7709	J033135−770900				
	PMN J0331−7719	J033138−772218				
SGRS J0400−8456.....	PMN J0401−8457	J040116−845642	04 01 18.4	−84 56 35.9	2.9	
		J040058−845449				
		J040058−845829				
		J035945−845530				
		J040145−850015				
SGRS J0515−8100.....	PMN J0515−8101	J051541−810139	05 15 55.0	−80 59 44.4	3.06	
		J051611−810219				
		J051653−810128				
		J051548−810314				
SGRS J0631−5405.....	PMN J0631−5405	J063159−540506	06 32 01.0	−54 04 58.7	37.7	
	MRC 0630−540	J063214−540405				
	1WGA J0631.9−5404	J063222−540320				
		J063151−540540				
SGRS J0746−5702.....	PMN J0746−5703	J074615−570312	07 46 18.6	−57 02 59.1	36.4	
	PMN J0746−5702	J074631−570152				
	PMNM 074521.2−565530	J074602−570434				
SGRS J0810−6800.....	PMN J0810−6759	J081038−675911	08 10 55.1	−68 00 07.7	...	0.34
		J081121−680109				
		J081029−675855				
		J081131−680200				
SGRS J0843−7007.....	PMN J0843−7006	J084243−700653	08 43 05.9	−70 06 55.6	12.0	
		J084305−700655				
		J084331−700739				
		J084349−700729				
SGRS J1259−7737.....	PKS B1255−773	J125846−773924	12 59 09.0	−77 37 28.4	...	0.33
	PMN J1259−7736	J125931−773500				
		J125920−773623				
SGRS J1336−8019.....	PMN J1335−8016	J133600−801807	13 35 59.7	−80 18 05.1	8.6	
	PMN J1336−8022	J133601−801637				
		J133600−801428				
		J133624−802250				
SGRS J1728−7237.....	PMN J1728−7237	J172828−723732	17 28 28.1	−72 37 34.9	11.9	
		J172806−723549				
		J172859−724011				
SGRS J1911−7048.....		J191052−704906	19 10 55.2	−70 49 00.9	1.2	
		J191120−704716				
		J191025−705110				
SGRS J1919−7959.....	PKS B1910−800	J191903−795741	19 19 16.9	−79 59 34.9	2.6	
	PMN J1918−7957	J191932−800145				
	MRC 1910−800	J191856−795651				
SGRS J1946−8222.....	PMN J1946−8221	J194640−822234	19 46 50.5	−82 22 53.8	2.1	
		J194552−822037				
		J194818−822539				
SGRS J2159−7219.....	PMN J2159−7220	J215908−721904	21 59 10.1	−72 19 06.6	9.6	
		J215918−722013				
		J215947−722203				
		J215827−721528				

Note.—Units of right ascension are hours, minutes, and seconds, and units of declination are degrees, arcminutes, and arcseconds.

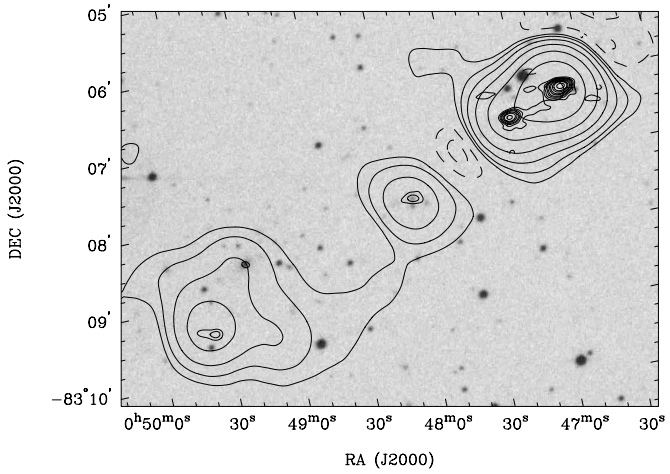

FIG. 1.—Radio-optical overlay of SGRS J0047−8307. The 843 MHz contours for the low-resolution SUMSS images are shown by thick lines, and 1.4 GHz contours for the higher resolution ATCA images are shown by thin lines. The radio contours are overlaid on the red SSS optical field, shown using gray scale. Contours are at −2, −1, 1, 2, 4, 8, 16, 32, and 64 × 4 mJy beam^{-1} for SUMSS and at −2, −1, 1, 2, 3, 4, 6, 8, 12, 16, and 24 × 3 mJy beam^{-1} for ATCA. The beams have FWHMs of 45″.2 × 45″ (SUMSS) and 8″.6 × 5″.9 (ATCA).

close neighbor ∼10″ to the southwest. There is a prominent halo associated with the host galaxy that appears asymmetric in the blue image, with an extension to the north.

5.1.6. *SGRS J0400−8456 (Fig. 6)*

The SUMSS image shows several emission peaks that are not all collinear. The ATCA image shows a central source coincident with a galaxy; this radio core has twin jets on either side (Fig. 6*b*). The SUMSS peaks to the north and south of the central component have compact features in the ATCA images. In the SUMSS image there is an extension from the northern peak toward the west that is oriented nearly orthogonal to the inner radio axis. There is a similar bend in the southern lobe toward the southeast. Compact structure is seen associated with the southernmost component in the high-resolution ATCA image. There is no optical identification at this location. We are not certain whether this component is a part of the giant radio galaxy and do not include it in the size determination. A low-resolution 1.4 GHz ATCA image made using the 1.5 km array is shown Figure 6*c*; the connectedness of the different components of the source is seen more clearly in this image. We have conservatively estimated the angular size to be the sky angle between the outer components of the source in Figure 6*c*. The source is edge-darkened; it is also one of the lowest power sources in the sample, and the source may be classified as FR I type. The multiple peaks on either side of the core have *Z*-symmetry: this is suggestive of multiple activity episodes in a precessing jet. The host is a relatively bright $b_J = 16.9$ galaxy with several close neighbors within a 1′ radius.

5.1.7. *SGRS J0515−8100 (Fig. 7)*

This double radio source has extremely low surface brightness lobes that have an extremely low axial ratio; the higher resolution ATCA observations have detected a faint radio core coincident with a galaxy that is located at the inner end of the southern lobe (Fig. 7*b*). There is an emission gap between the core and the northern lobe. This source appears to be a giant fat double radio source and is being studied in detail by R. Subrahmanyan et al. (2005, in preparation). The optical spectrum of the host galaxy was obtained by Vincent McIntyre and Carole Jackson in 1999 using the DBS at the Siding Spring Observatory (SSO) 2.3 m telescope.

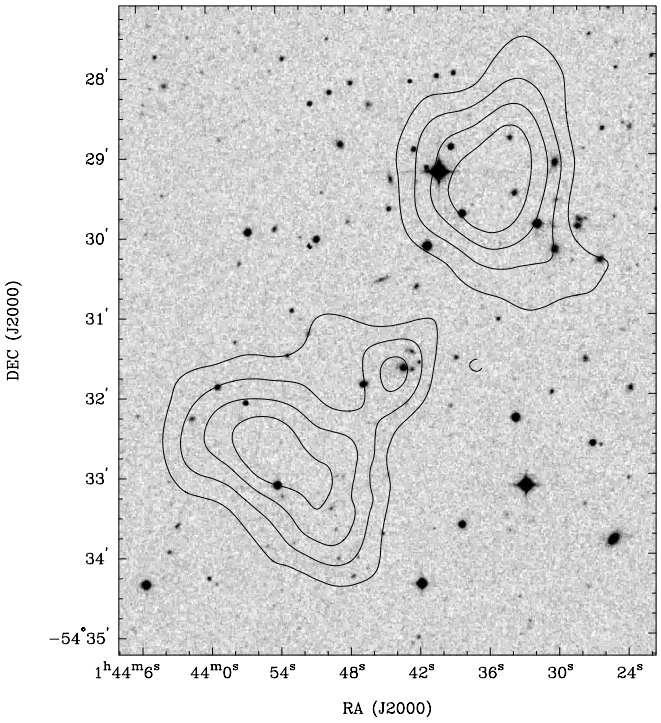

FIG. 2*a*

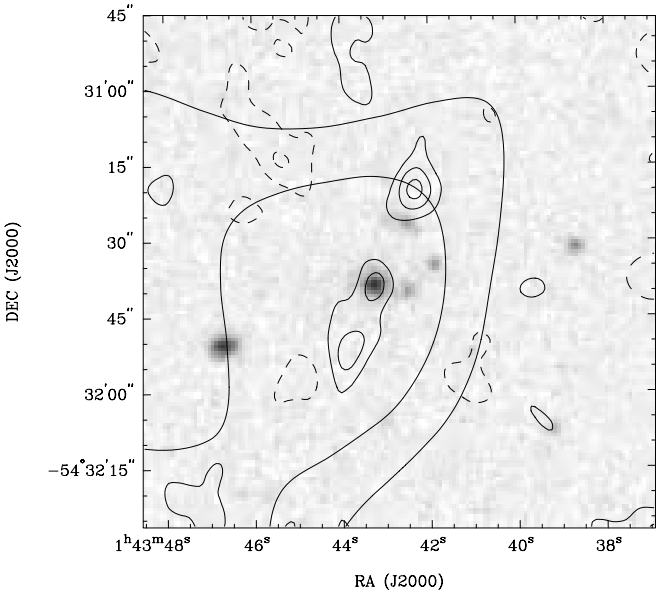

FIG. 2*b*

FIG. 2.—(*a*) SGRS J0143−5431 radio contours on the blue SSS gray scale. SUMSS contours (*thick lines*) are at −2, −1, 1, 2, 3, and 4 × 4 mJy beam^{-1}, and ATCA contours (*thin lines*) are at −2, −1, 1, 2, and 3 × 0.7 mJy beam^{-1}. (*b*) Zoom of the region close to the core. The beams have FWHMs of 54″.3 × 45″ (SUMSS) and 8″.5 × 7″.2 (ATCA).

5.1.8. *SGRS J0631−5405 (Fig. 8)*

This giant radio source is a quasar. The SUMSS image shows a pair of lobes; the higher resolution ATCA image shows a strong radio core coincident with a starlike object. The ATCA image shows compact structure at the end of the western lobe, whereas

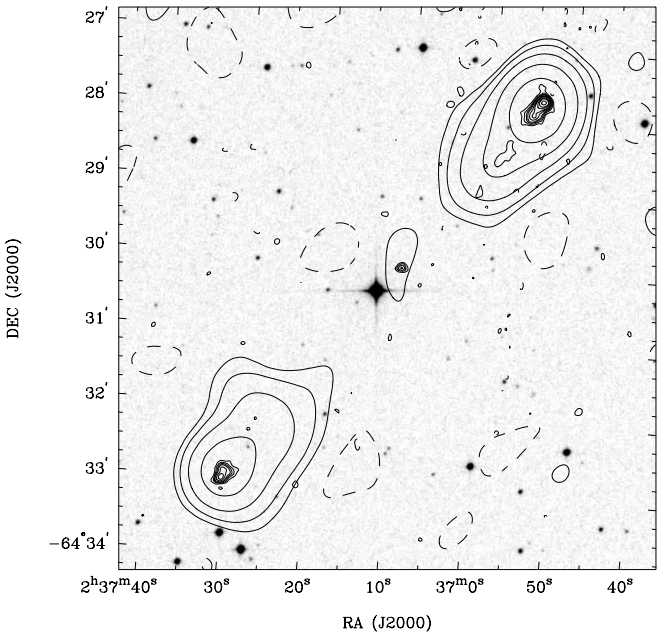

FIG. 3.—GRS J0237−6429 radio contours on the blue SSS gray scale. SUMSS contours (*thick lines*) are at −2, −1, 1, 2, 4, 8, and 16 × 2 mJy beam^{-1}, and ATCA contours (*thin lines*) are at −2, −1, 1, 2, 3, 4, 6, 8, 12, 16, and 24 × 2 mJy beam^{-1}. The beams have FWHMs of 50.″1 × 45″ (SUMSS) and 7.″6 × 7.″3 (ATCA).

the eastern lobe appears resolved. The western lobe has a smaller extent from the core and also has a higher surface brightness. There is an emission gap between the core and the lower surface brightness eastern lobe. The quasar has been cataloged in the Deep X-Ray Radio Blazar Survey (Perlman et al. 1998) and is a known X-ray source in the *ROSAT* PSPC database of point sources.

5.1.9. *SGRS J0746−5702 (Fig. 9)*

In the SUMSS, this radio source appears as a bright extended central source flanked by much fainter lobes. In the higher resolution ATCA image the central source is resolved into a strong core and a jetlike feature to the southwest. Both lobes are resolved in the ATCA observations, and no compact structure is observed. The jet appears directed toward the fainter of the two lobes. The radio structure at 843 MHz can be classified as FR I type given the edge-darkened lobes; however, the detection of a one-sided partial jet some distance from the core is unusual and indicates that this source might be another example of a restarting jet within relict lobes. There is a neighboring galaxy situated ∼4″ from the host galaxy at a position angle perpendicular to the radio axis of the source.

5.1.10. *SGRS J0810−6800 (Fig. 10)*

The SUMSS image shows two lobes; the northwestern lobe is edge-brightened and has the higher surface brightness. A compact source is detected at the peak of the northwestern lobe in the ATCA 1.4 GHz image; the southeastern lobe is completely resolved. The ATCA image at 4.8 GHz (Fig. 10*b*) reveals a faint radio core coincident with a starlike object that is located on the line joining the outer ends of the two lobes. The lobes do not, however, extend along this line and appear to be directed to the north of the axis in both cases. The host object has very broad Hβ and Hα emission lines and is a quasar. The host object is starlike in blue; however, in the red SSS images it is surrounded by three faint patches of emission. An unusual aspect of this giant radio source is that although it has a broad-line host, the radio core is weak. An unusual feature of the spectrum is the associated

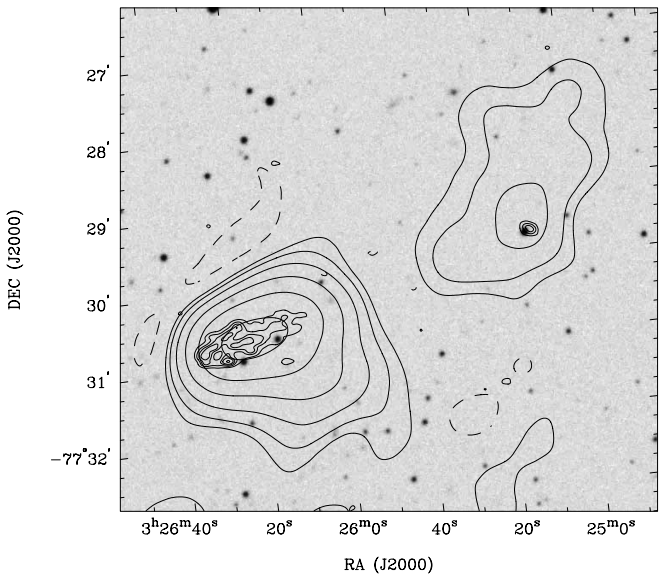

FIG. 4*a*

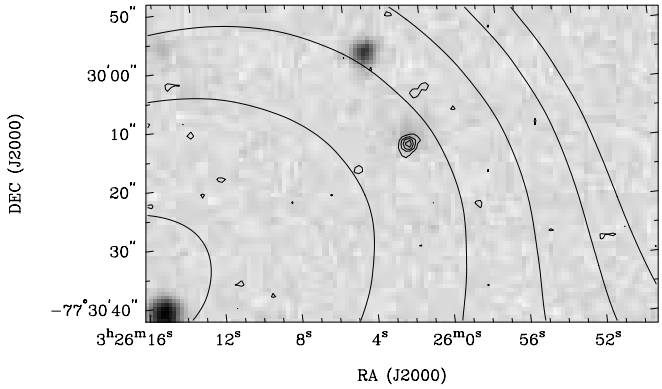

FIG. 4*b*

FIG. 4.—SGRS J0326−7730 radio contours on the red SSS gray scale. A zoom of the core region is shown in (*b*), in which 4.8 GHz ATCA contours are shown by thin lines. SUMSS contours (*thick lines*) are at −2, −1, 1, 2, 4, 8, 16, and 32 × 3 mJy beam^{-1}, and ATCA contours (*thin lines*) are at −2, −1, 1, 2, 3, 4, and 6 × 0.7 mJy beam^{-1} for the 1.4 GHz image and at −2, −1, 1, 2, 3, and 4 × 0.1 mJy beam^{-1} for the 4.8 GHz image. The beams have FWHMs of 46.″4 × 45″ (SUMSS), 7.″8 × 4.″9 (ATCA, 1.4 GHz), and 2.″2 × 1.″8 (ATCA, 4.8 GHz).

blueshifted absorption in the Balmer lines, indicating the presence of recent star formation.

5.1.11. *SGRS J0843−7007 (Fig. 11)*

The radio structure of this giant radio source resembles SGRS J0746−5702 in that it has a central, bright component straddled by two extended lobes with low surface brightness. In the higher resolution ATCA image only a central radio core is detected; the two low surface brightness lobes are completely resolved. The host galaxy has a close neighbor ∼10″ to the north. This source might be a relict of a giant FR II radio source in which the beams from the central engine no longer energize the lobes.

5.1.12. *SGRS J1259−7737 (Fig. 12)*

This giant radio source has prominent lobes and is clearly seen to be an edge-brightened double radio source. The two lobes extend all the way toward each other without any emission gap. The 1.4 GHz ATCA high-resolution image detected compact

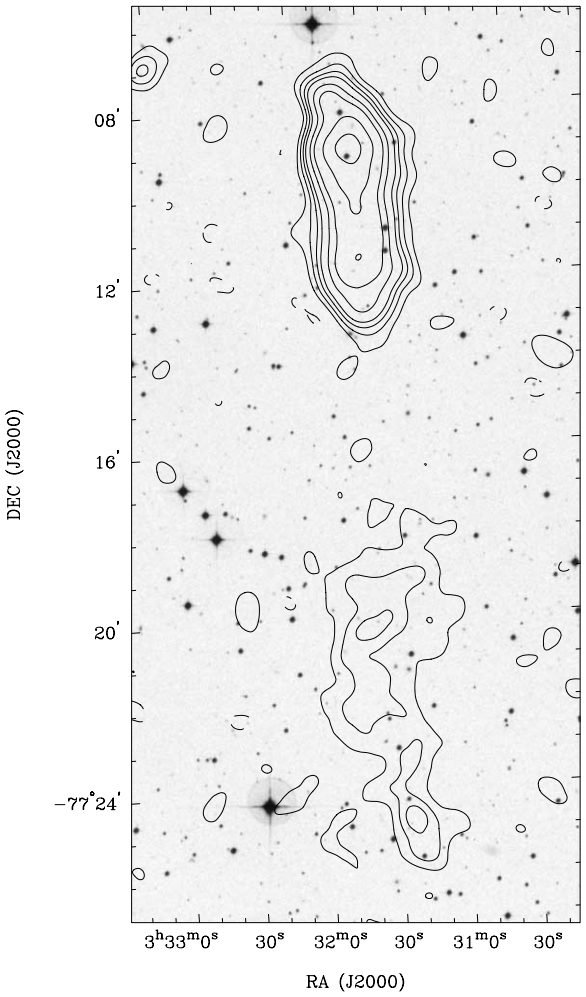

FIG. 5*a*

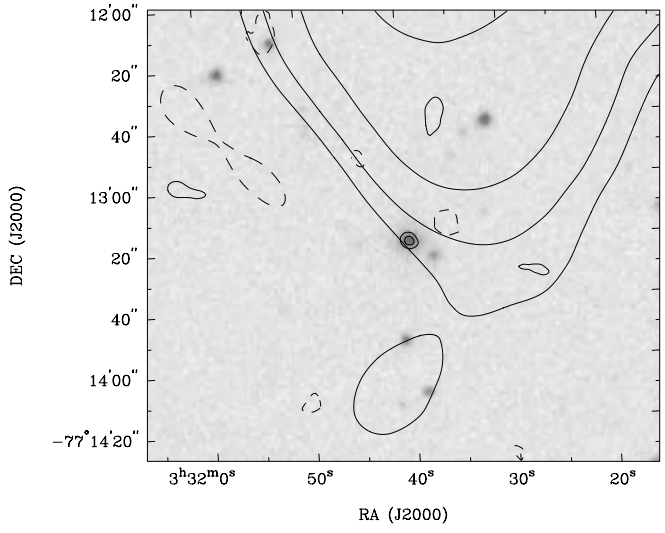

FIG. 5*b*

FIG. 5.—SGRS J0331−7710 radio contours on the blue SSS gray scale. A zoom of the core region is shown in (*b*). SUMSS contours (*thick lines*) are at (*a*) −2, −1, 1, 2, 3, 4, 6, 8, 12, and 16 × 2 mJy beam^{-1} and at (*b*) −1, 1, 2, 4, and 8 × 3 mJy beam^{-1}; ATCA contours (*thin lines*) are at −1, 1, and 1.5 × 0.8 mJy beam^{-1}. The beams have FWHMs of 46.″4 × 45″ (SUMSS) and 9.″1 × 6″ (ATCA).

hot spots at the ends of both lobes, and later 4.8 GHz ATCA imaging detected an additional weak compact core close to the center of the radio source (Fig. 12*b*). The core is coincident with a faint object at the plate limit. The sky region in which the host galaxy lies appears relatively devoid of optical objects, suggesting dust obscuration along this line of sight. In spite of a 5 × 2000 s exposure on the 2.3 m telescope, we were unable to obtain a firm redshift for this galaxy because of its faintness. A *K*-band image of the field was obtained for us by Helen Johnston with the Cryogenic Array Spectrometer/Imager (CASPIR) on the ANU 2.3 m telescope at SSO. A host galaxy is clearly detected at the location of the radio core. We estimate its *K* magnitude to be 16.2 ± 0.2; using the *K*-*z* relation for radio galaxies, we estimate its redshift to be >0.3. Its linear size is estimated to be >1.5 Mpc.

5.1.13. *SGRS J1336−8019 (Fig. 13)*

In the SUMSS this double radio source appears to have an edge-brightened structure with a high axial ratio. The higher resolution ATCA image shows a chain of weak compact features that trace the chain of peaks observed in SUMSS, indicating the presence of a weak two-sided jet along the central line of this radio source. The strongest among the emission peaks is the central core component, and this coincides with the southern member of a close pair of objects (Fig. 13*b*) that were partly blended on the spectrograph slit. The presence of Hα absorption at rest in the host galaxy spectrum indicates that the northern object is a star. The ATCA image also detects a feature at the leading edge of the southern lobe; however, there is no recognizable equivalent feature at the leading edge of the northern lobe.

5.1.14. *SGRS J1728−7237 (Fig. 14)*

The source is a triple in both the SUMSS and ATCA images. There are large emission gaps between the lobes and the core. This is an asymmetric source with the northern lobe closer to the core as compared to the southern lobe. The ATCA image detects a radio core that is displaced ∼7″ from a bright star and coincident with a faint galaxy, which has a prominent narrow emission-line spectrum. There are several faint galaxies visible in the neighborhood of the host.

5.1.15. *SGRS J1911−7048 (Fig. 15)*

The large-scale radio structure indicates a low surface brightness edge-brightened radio source with a continuous bridge connecting the two lobes. In the higher resolution ATCA image only a core is detected at the center of the source and coincident with a faint galaxy; the rest of the lobe structure is completely resolved.

5.1.16. *SGRS J1919−7959 (Fig. 16)*

This giant radio source was observed earlier by Subrahmanyan et al. (1996). The SUMSS image shows a pair of prominent lobes; the ATCA image detects structure in both these lobes. In addition, the ATCA image from Subrahmanyan et al. (1996) detects a weak core between the two lobes and coincident with a faint $b_J = 22.7$ galaxy. Inspection of the digitized plates reveals significant dust obscuration. The optical spectrum was obtained by R. W. H. in 1994 using the Faint Object Red Spectrograph on the Anglo-Australian Telescope.

5.1.17. *SGRS J1946−8222 (Fig. 17)*

The high-resolution ATCA image of this source shows a compact, weak core component coincident with a faint host galaxy; the core is straddled by a pair of partial jetlike features that are symmetrically located on either side of the core. The SUMSS image shows extended emission around this central structure as

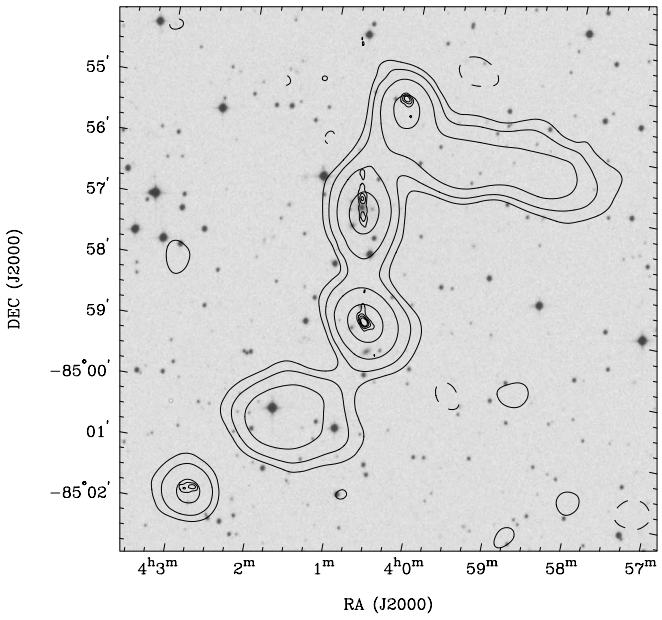

FIG. 6*a*

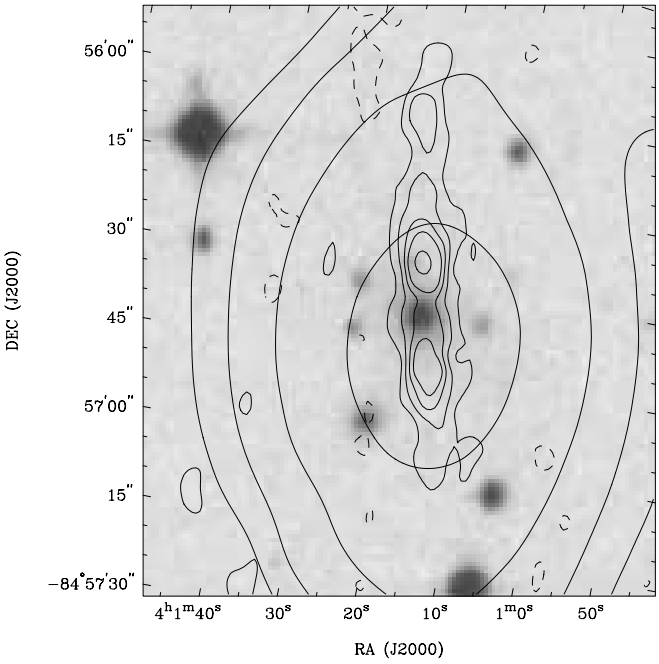

FIG. 6*b*

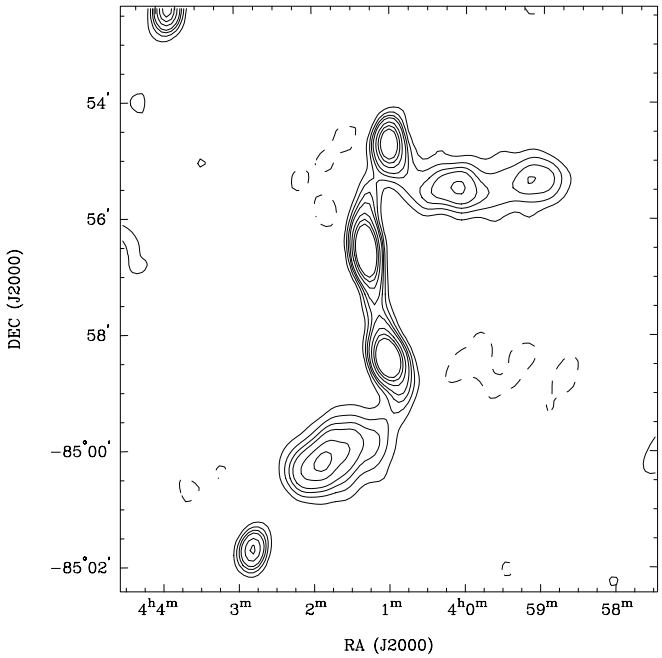

FIG. 6*c*

FIG. 6.—SGRS J0400−8456 radio contours on the blue SSS gray scale. A zoom of the core region is shown in (*b*). SUMSS contours (*thick lines*) are at (*a*) −1, 1, 2, 4, and 8×2 mJy beam^{-1} and at (*b*) −1, 1, 2, 4, and 8×3 mJy beam^{-1}; ATCA contours (*thin lines*) are at (*a*) −1, 1, 2, 3, and 4×1 mJy beam^{-1} and at (*b*) −1, 1, 2, 3, 4, and 6×0.1 mJy beam^{-1}. The beams have FWHMs of $45\farcs2 \times 45''$ (SUMSS) and $8\farcs1 \times 4\farcs7$ (ATCA). (*c*) Low-resolution 1.4 GHz ATCA image of SGRS J0400−8456. The contours are at −2, −1, 1, 2, 3, 4, 6, 8, 10×0.8 mJy beam^{-1}. The beam FWHM is $34'' \times 21''$.

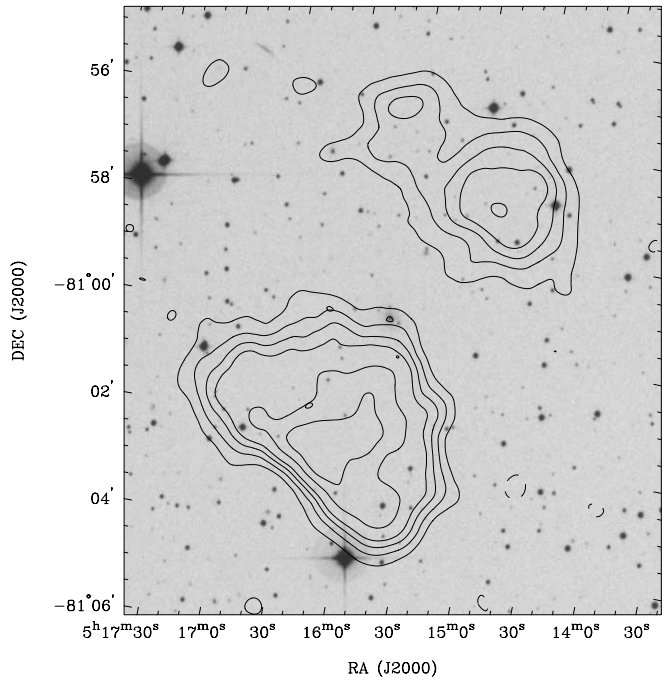

FIG. 7*a*

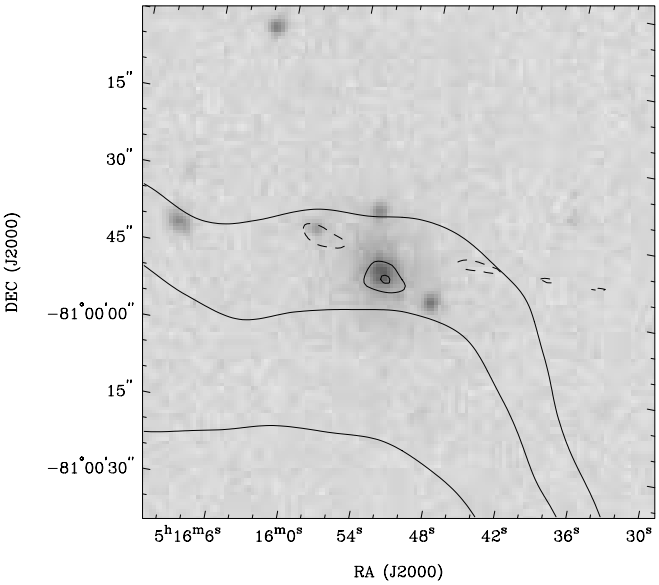

FIG. 7*b*

FIG. 7.—SGRS J0515−8100 radio contours on the blue SSS gray scale. A zoom of the core region is shown in (*b*). SUMSS contours (*thick lines*) are at −1, 1, 2, 3, 4, 6, and 8 × 1.5 mJy beam^{-1}, and ATCA contours (*thin lines*) are at (*a*) 2 mJy beam^{-1} and at (*b*) −1, 1, and 2 × 1 mJy beam^{-1}. The beams have FWHMs of 45″.7 × 45″ for SUMSS and (*a*) 8″.5 × 6″.1 and (*b*) 7″.1 × 5″ for ATCA.

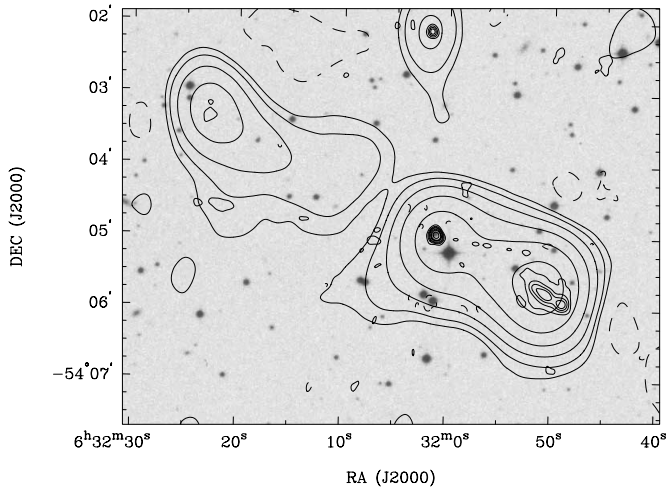

FIG. 8.—SGRS J0631−5405 radio contours on the blue SSS gray scale. SUMSS contours (*thick lines*) are at −1, 1, 2, 4, 8, 16, and 32 × 4 mJy beam^{-1}, and ATCA contours (*thin lines*) are at −1, 1, 2, 3, 4, 6, 8, and 12 × 2.5 mJy beam^{-1}. The beams have FWHMs of 54″.3 × 45″ (SUMSS) and 8″.5 × 7″.3 (ATCA).

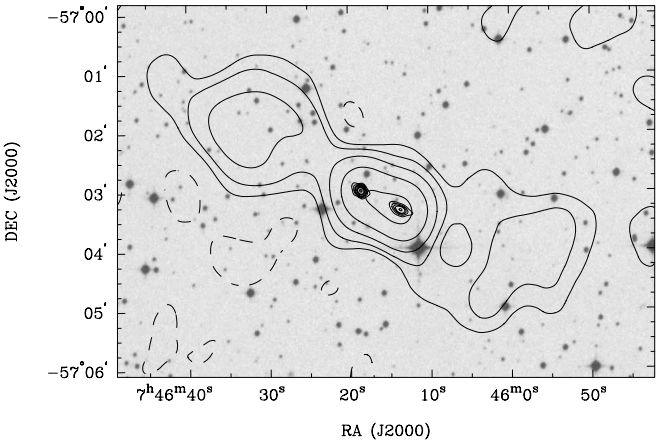

FIG. 9.—SGRS J0746−5702 radio contours on the blue SSS gray scale. SUMSS contours (*thick lines*) are at −1, 1, 2, 4, 8, and 16 × 3 mJy beam^{-1}, and ATCA contours (*thin lines*) are at −1, 1, 2, 3, 4, 6, 8, and 12 × 3 mJy beam^{-1}. The beams have FWHMs of 54″.3 × 45″ (SUMSS) and 8″.4 × 7″.1 (ATCA).

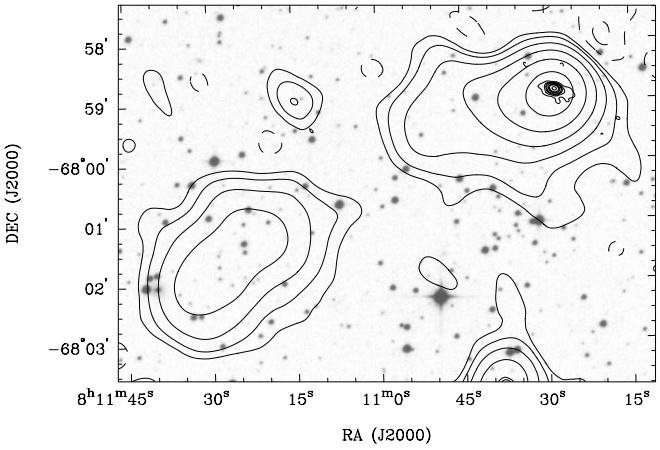

FIG. 10*a*

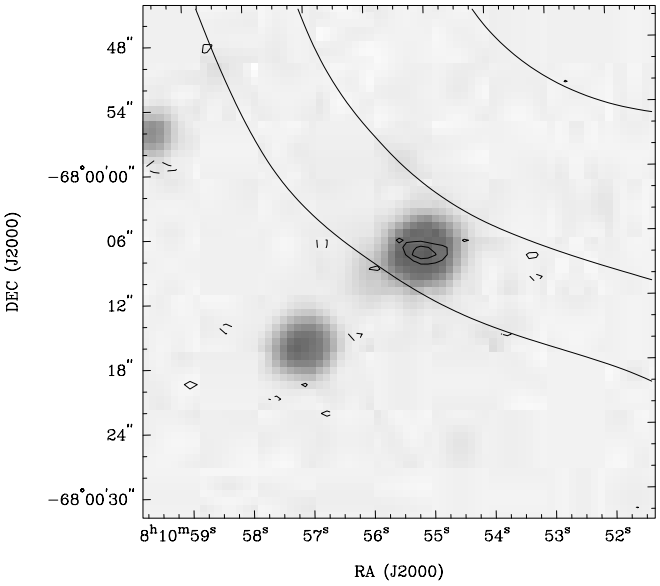

FIG. 10*b*

FIG. 10.—SGRS J0810−6800 radio contours on the red SSS gray scale. The core region is shown in (*b*) with 4.8 GHz contours plotted as thin lines. SUMSS contours (*thick lines*) are at −1, 1, 2, 4, 8, 16, and 32×1.5 mJy beam^{-1}. ATCA contours (*thin lines*) are at −1, 1, 2, 3, 4, 6, 8, and 12×1.5 mJy beam^{-1} for the 1.4 GHz image and at −1, 1, 2×0.1 mJy beam^{-1} for the 4.8 GHz image. The beams have FWHMs of $48''.5 \times 45''$ (SUMSS), $9''.3 \times 6''.1$ (ATCA, 1.4 GHz), and $3''.4 \times 1''.4$ (ATCA, 4.8 GHz).

two lobes that have a high axial ratio. The two ends of the source are asymmetrically located with respect to the core. There are no prominent compact hot spots seen at the ends of the source in the 1.4 GHz ATCA image. The inner partial jets might be a case of restarting beams in this giant radio source. The host galaxy is barely seen in the blue, while in the red the host appears as a pointlike feature with faint extended optical emission. We twice attempted to obtain a redshift for this galaxy, but poor observing conditions allowed for only a tentative estimate.

5.1.18. *SGRS J2159−7219 (Fig. 18)*

In the SUMSS this source has an edge-brightened outer structure and a central triple structure with emission gaps between all components. There is a larger emission gap between the northern lobe and the core. In the ATCA 1.4 GHz image a compact radio core is detected at the location of the central component, and this coincides with a bright galaxy (Fig. 18*b*). At this higher frequency and resolution the only other structure seen is the stronger southern component of the central triple. The host galaxy has a prominent halo; fainter companions are seen in its neighborhood, and the host is likely to be in a cluster environment. The optical spectrum was obtained by Boyce (2000).

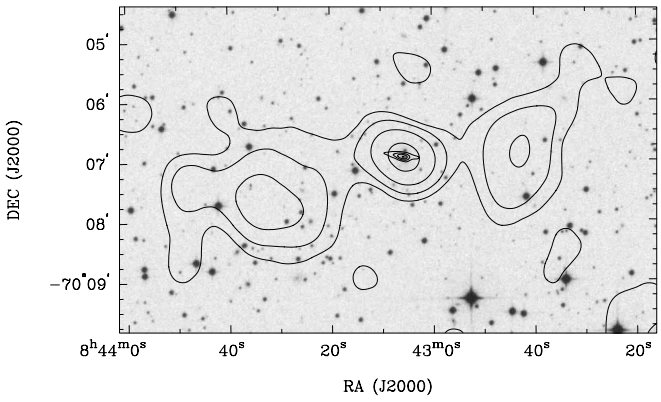

FIG. 11.—SGRS J0843−7007 radio contours on the blue SSS gray scale. SUMSS contours (*thick lines*) are at −1, 1, 2, 4, and 8×3 mJy beam^{-1}, and ATCA contours (*thin lines*) are at −1, 1, 2, 3, and 4×3 mJy beam^{-1}. The beams have FWHMs of $47''.3 \times 45''$ (SUMSS) and $9''.5 \times 6''$ (ATCA).

6. DISCUSSION

SUMSS has an rms noise of about 1 mJy beam^{-1} and a 5 σ surface brightness detection limit of about 12 mJy arcmin^{-2}. With a beam that has a FWHM close to $1'$, it is the best survey today for finding low-redshift giant radio sources in the southern sky. The sample of giant radio sources that we have compiled from SUMSS and presented in this paper is the only complete sample in the south.

We find 18 giant radio sources in the 2100 deg^2 of the search area. There are four giant radio sources in this sample with redshifts $z \leq 0.13$; these are in the comoving search volume of 3.5×10^7 Mpc^3 for which the survey is expected to detect all edge-brightened giant radio sources with projected linear size exceeding 0.7 Mpc. This implies that the space density of giant radio galaxies is about 10^{-7} Mpc^{-3} at the survey sensitivity, or that a giant radio source is expected for every (215 Mpc)^3 in the local universe.

The space density of powerful FR II radio sources in the local universe is about 10^{-7} Mpc^{-3} (Padovani & Urry 1992). Of the four giant radio sources we detect at $z \leq 0.13$, SGRS J0400−8456 is an FR I radio galaxy, while the remaining three (SGRS J0515−8100, J0746−5702, and J2159−7219) are sources with relaxed—possibly relict—lobes and have radio luminosities significantly below the FR I/FR II break luminosity of 1.3×10^{25} W Hz^{-1}. None of the giant radio galaxies in our sample at $z \leq 0.13$ is a classic powerful radio source; none of them have hot spots within the lobes, and none of them are above the FR I/FR II break in radio luminosity. Within the comoving search volume of 3.5×10^7 Mpc^3, where the survey is expected to detect all edge-brightened giant radio sources with projected linear size

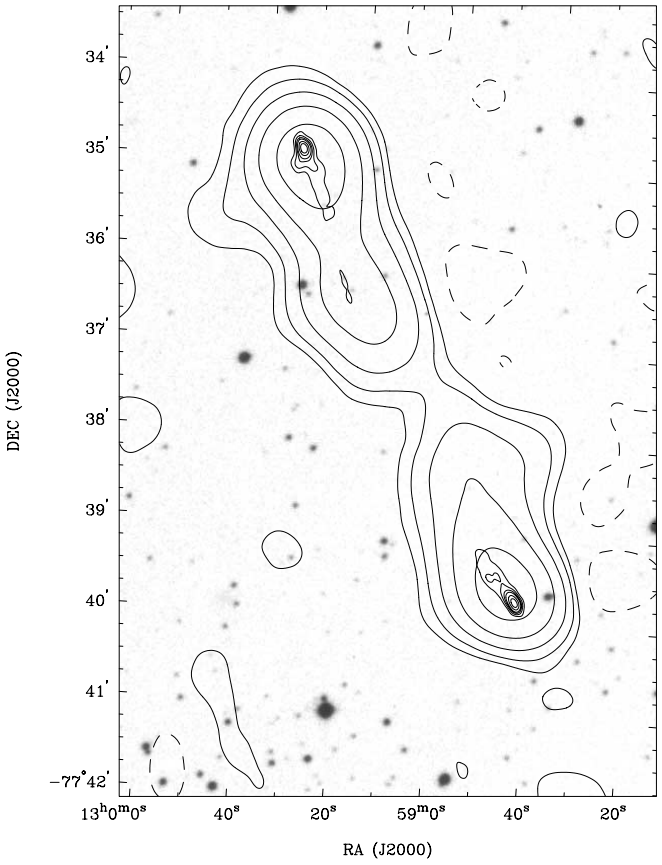

FIG. 12*a*

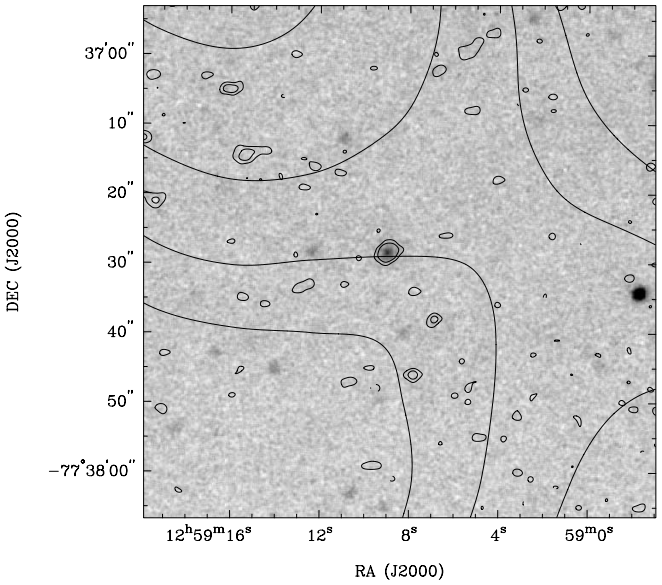

FIG. 12*b*

FIG. 12.—SGRS J1259−7737 radio contours. A blue SSS gray scale image is shown in (*a*), and an SSO 2.3 m *K*-band image in gray scale is shown in (*b*). The *K*-band image was obtained by H. Johnston. The core region is shown in (*b*), with 4.8 GHz contours shown using thin lines. SUMSS contours (*thick lines*) are at −1, 1, 2, 4, 8, and 16 × 4 mJy beam^{-1}, and ATCA contours (*thin lines*) are at −1, 1, 2, 3, 4, 6, and 8 × 3 mJy beam^{-1} for the 1.4 GHz image and at −1, 1, and 2 × 0.07 mJy beam^{-1} for the 4.8 GHz image. The beams have FWHMs of 46.″4 × 45″ (SUMSS), 9.″4 × 5.″8 (ATCA, 1.4 GHz), and 2.″2 × 1.″8 (ATCA, 4.8 GHz).

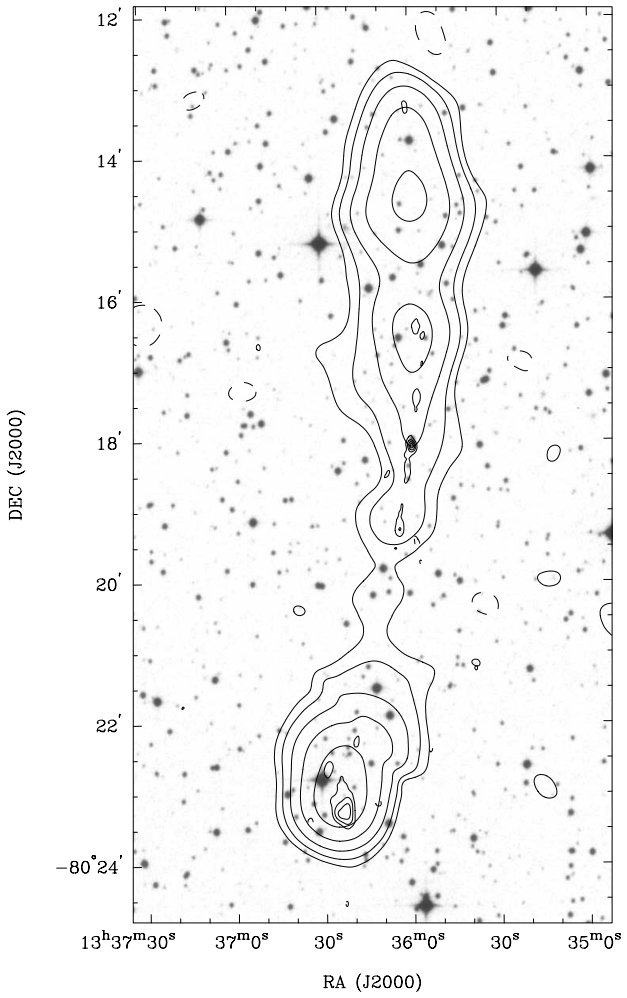

FIG. 13*a*

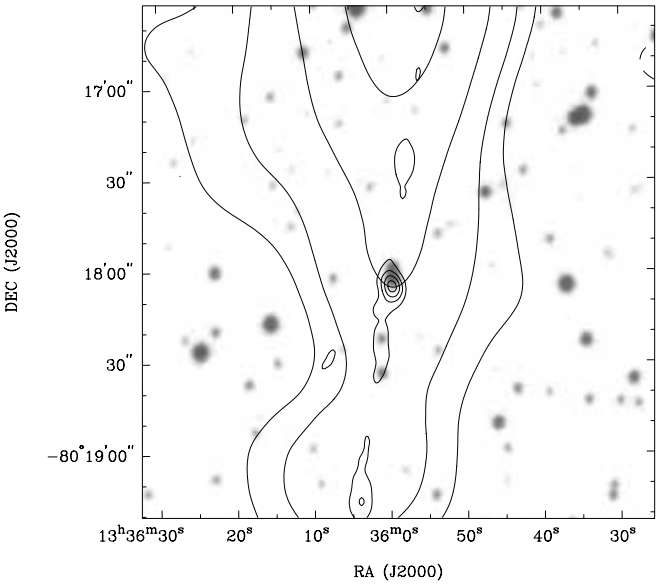

FIG. 13*b*

FIG. 13.—SGRS J1336−8019 radio contours on the blue SSS gray scale. A zoom of the core region is shown in (*b*). SUMSS contours (*thick lines*) are at −1, 1, 2, 4, 8, and 16 × 3 mJy beam^{-1}, and ATCA contours (*thin lines*) are at −1, 1, 2, 3, and 4 × 2 mJy beam^{-1}. The beams have FWHMs of 45.″7 × 45″ (SUMSS) and 9.″3 × 5.″8 (ATCA).

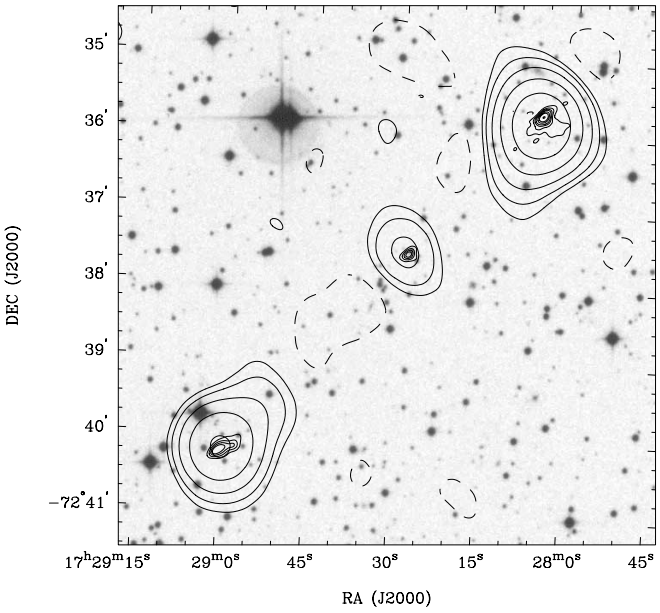

FIG. 14.—SGRS J1728−7237 radio contours on the blue SSS gray scale. SUMSS contours (*thick lines*) are at −1, 1, 2, 4, 8, and 16 × 3 mJy beam^{-1}, and ATCA contours (*thin lines*) are at −1, 1, 2, 3, 4, 6, 8, and 12 × 2.5 mJy beam^{-1}. The beams have FWHMs of 47″.3 × 45″ (SUMSS) and 8″.9 × 6″.1 (ATCA).

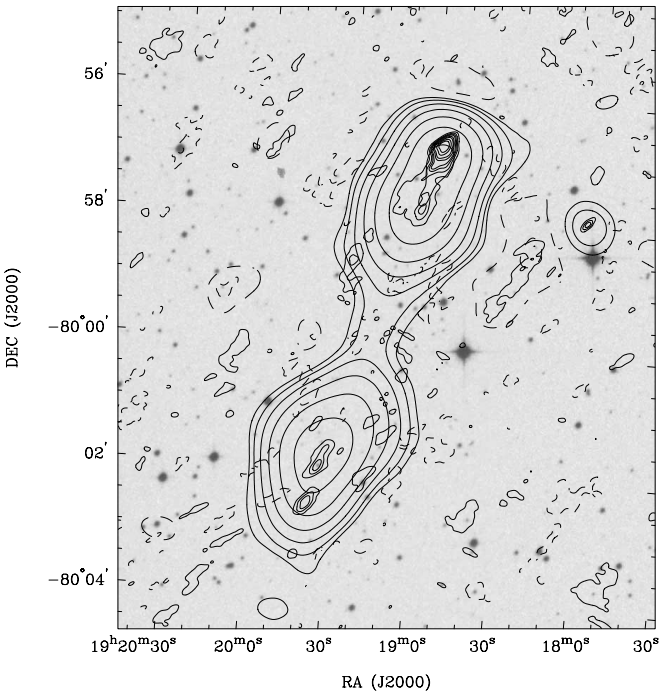

FIG. 16.—SGRS J1919−7959 radio contours on the red SSS gray scale. SUMSS contours (*thick lines*) are at −1, 1, 2, 4, 8, 16, 32, and 64 × 4 mJy beam^{-1}, and ATCA contours (*thin lines*) are at −1, 1, 2, 3, 4, 6, 8, 12, and 16 × 2 mJy beam^{-1}. The beams have FWHMs of 45″.7 × 45″ (SUMSS) and 11″.8 × 5″.1 (ATCA).

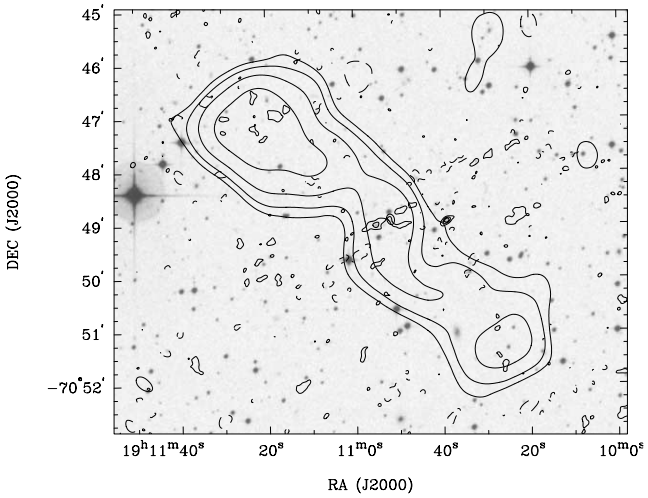

FIG. 15.—SGRS J1911−7048 radio contours on the blue SSS gray scale. SUMSS contours (*thick lines*) are at −1, 1, 2, 4, and 8 × 2 mJy beam^{-1}, and ATCA contours (*thin lines*) are at −1, 1, and 2 × 0.5 mJy beam^{-1}. The beams have FWHMs of 47″.3 × 45″ (SUMSS) and 9″.8 × 5″.9 (ATCA).

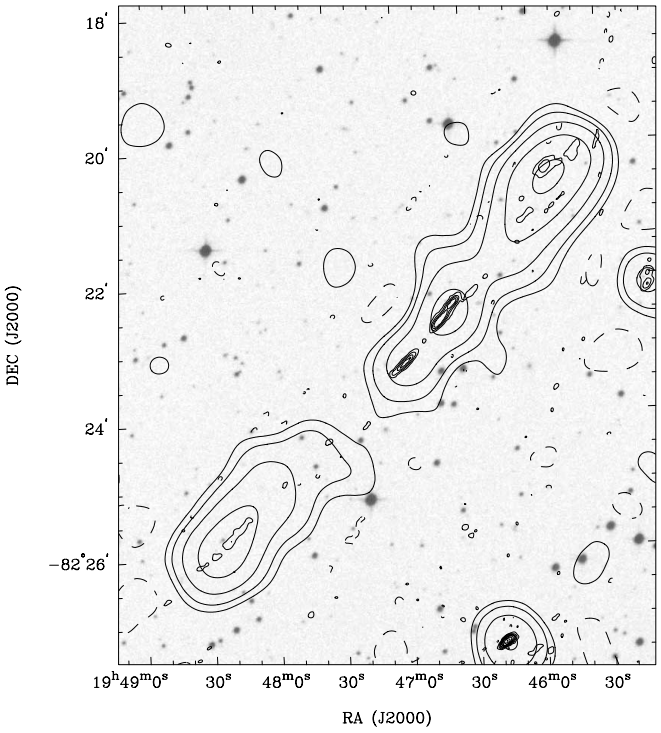

FIG. 17.—SGRS J1946−8222 radio contours on the red SSS gray scale. SUMSS contours (*thick lines*) are at −1, 1, 2, 4, 8, and 16 × 2 mJy beam^{-1}, and ATCA contours (*thin lines*) are at −1, 1, 2, 3, 4, 6, 8, 12, and 16 × 0.6 mJy beam^{-1}. The beams have FWHMs of 45″.2 × 45″ (SUMSS) and 10″.2 × 4″.3 (ATCA).

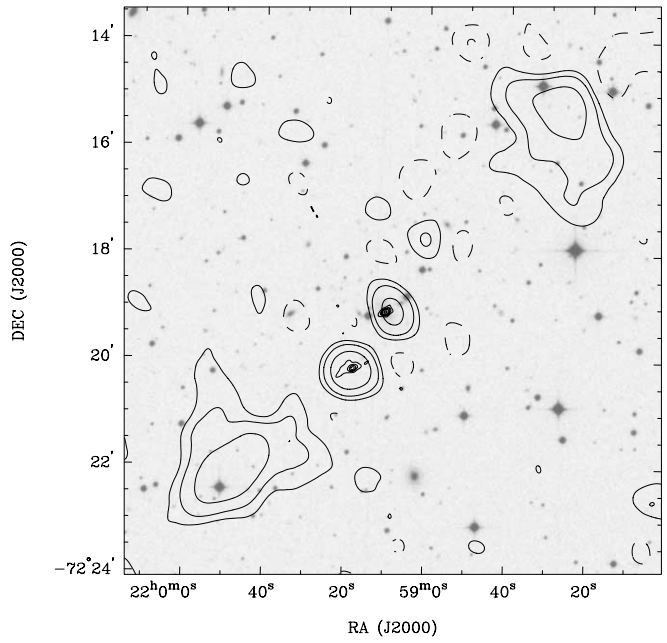

FIG. 18*a*

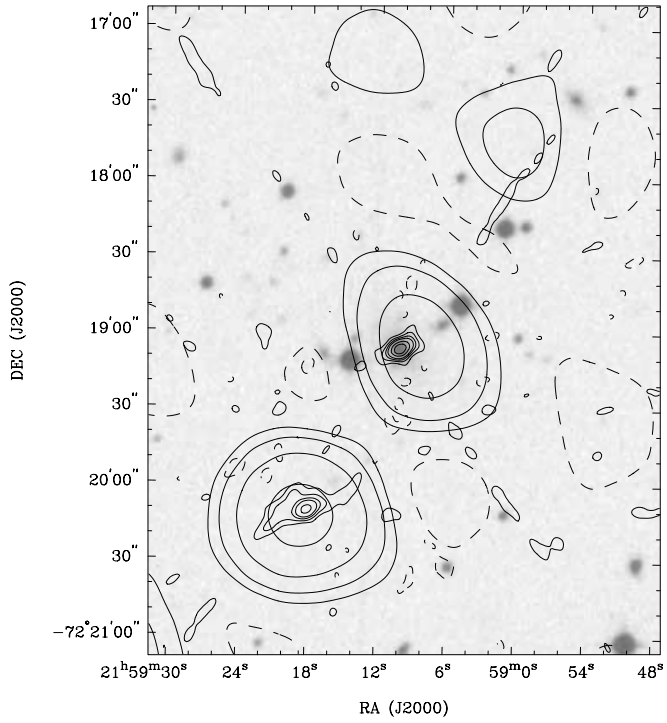

FIG. 18*b*

FIG. 18.—SGRS J2159−7219 radio contours on the blue SSS gray scale. A zoom of the core region is shown in (*b*). SUMSS contours (*thick lines*) are at −1, 1, 2, and 4 × 2.5 mJy beam^{-1}, and ATCA contours (*thin lines*) are at −1, 1, 2, 3, 4, and 6 × 1.5 mJy beam^{-1} in (*a*). In (*b*), SUMSS contours are at −1, 1, 2, 4, and 8 × 2 mJy beam^{-1}, and ATCA contours are at −1, 1, 2, 3, 4, 6, and 8 × 1 mJy beam^{-1}. The beams have FWHMs of 47″.3 × 45″ (SUMSS) and 9″.4 × 6″ (ATCA).

exceeding 0.7 Mpc, all the giants we detect have relict lobes, suggesting that *at low redshifts giant radio sources with relict lobes are more numerous than active giants in which the lobes are energized by beams from the center.* The lack of powerful edge-brightened giant radio sources in this survey volume is consistent with the expected small number of powerful edge-brightened radio sources given the small search region. It is likely that the giant radio sources we detect at $z \leq 0.13$—which have edge-brightened relict lobes—are relicts of FR II giant radio sources. The characteristics of these $z \leq 0.13$ sources allow us to make the tentative inference that FR II giant radio sources may have much shorter lifetimes in the active phase as compared to the time for which their fading relict lobes remain visible above the survey sensitivity limit.

Forty-six giant radio sources were found in the WENSS area of 8100 deg^2 north of declination $\delta = +28^\circ$ (Schoenmakers et al. 2001). The angular size and linear size cutoffs in the selection of WENSS giants were the same as the criteria we have adopted here. The WENSS sensitivity varied with declination; assuming that giant radio sources have a spectral index $\alpha = -0.7$ to -1.0 ($S_\nu \propto \nu^\alpha$), the WENSS has a sensitivity to these extended sources that is somewhat better than the SUMSS sensitivity in the sky north of $\delta = +74^\circ$ and comparable in most of the survey region $+28^\circ < \delta < +74^\circ$. In the 600 deg^2 where the surface brightness sensitivity in the WENSS is better, the detection rate in the WENSS search is a factor of 1.7 higher. However, in the 7500 deg^2 where the surface brightness sensitivity of the WENSS is comparable to that of the SUMSS, the detection rate in the WENSS is only 0.6 times that in our SUMSS-based search. It may be noted that Lara et al. (2001) have pointed out that as many as eight giant sources at $\delta > +60^\circ$ missed being selected in the compilation of Schoenmakers et al. (2001).

Barring two giant radio sources (SGRS J0400−8456 and SGRS J2159−7219), none of the SUMSS giant radio sources in the sample presented here are likely to belong to clusters. We examined their galaxy environments in the SSS fields and found them to be isolated, having close companions or being in a small group of galaxies.

Six of the 18 giant radio sources in the sample show classic FR II radio morphology with compact hot spots at each of the lobe ends (SGRS J0047−8307, J0237−6429, J0631−5405, J1259−7737, J1728−7237, and J1919−7959). SGRS J0810−6800 and SGRS J1336−8019 are FR IIs with compact structure at the end of only one lobe; in both these sources the ATCA images show no compact component in the other lobe.

SGRS J0326−7730 and SGRS J0331−7710 have large-scale SUMSS structures that are highly asymmetric in lobe flux density and lobe separation from their cores. Of these, SGRS J0326−7730 is observed to have structure at the end of one lobe in the ATCA image; SGRS J0331−7710 is not observed to have any compact structure in either lobe.

Seven sources show relaxed lobes with no compact hot spots at either end (SGRS J0143−5431, J0515−8100, J0746−5702, J0843−7007, J1911−7048, J1946−8222, and J2159−7219). All these seven sources with relaxed lobes are among the relatively low radio power sources in the sample; this is consistent with the interpretation that these are relict sources in which beams do not currently feed the outer relaxed lobes. Of these, SGRS J0143−5431, J0746−5702, J1946−8222, and J2159−7219 have evidence for either one- or two-sided knots/jets closer to the nucleus and might be examples of giant radio sources with relict lobes and restarting beams.

SGRS J0400−8456 is the only source in the sample that is observed to have highly bent tail-like lobe structures that decrease

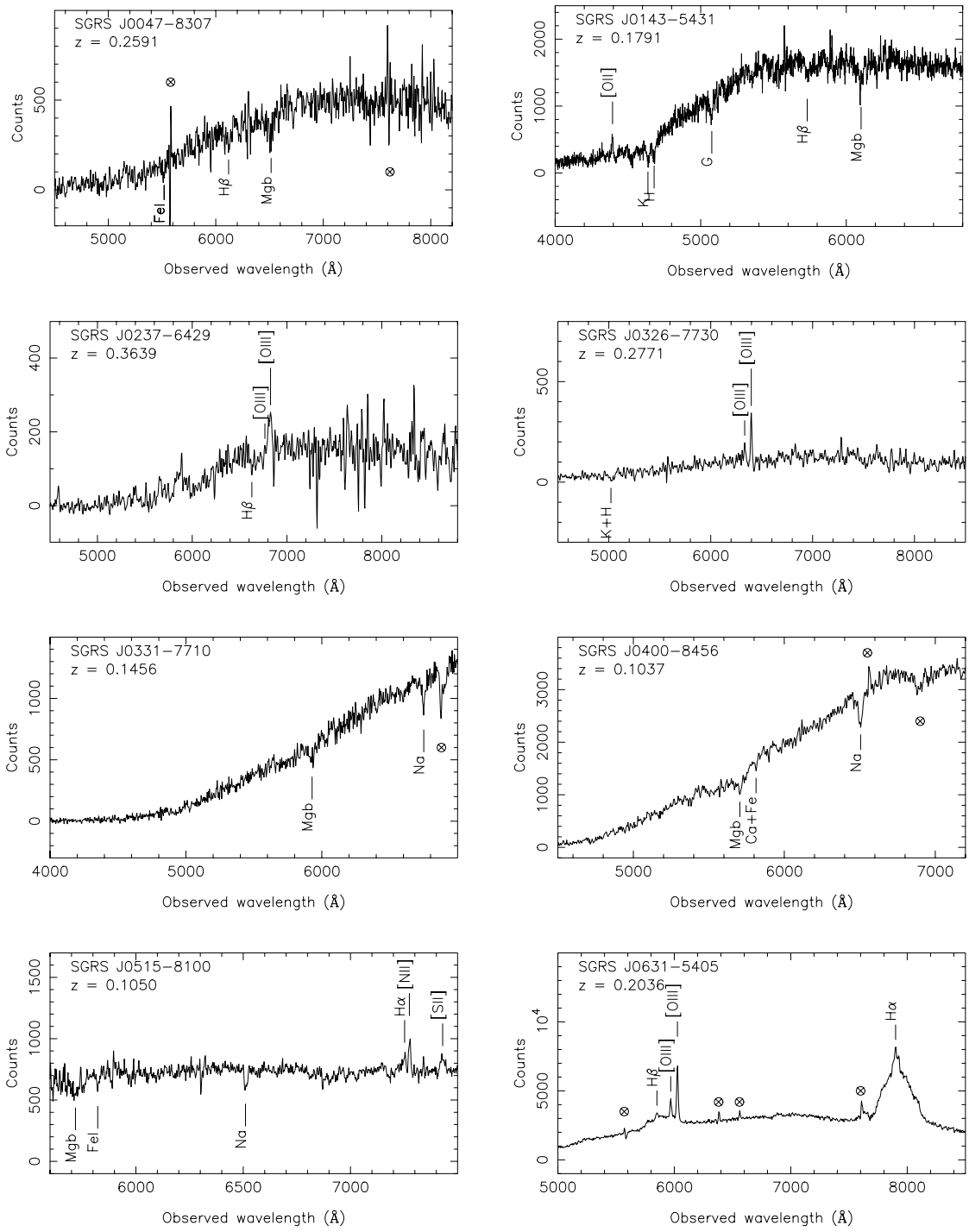

FIG. 19.—Optical spectra of the complete sample of giant radio sources. The circled crosses represent features that we consider to be artifacts.

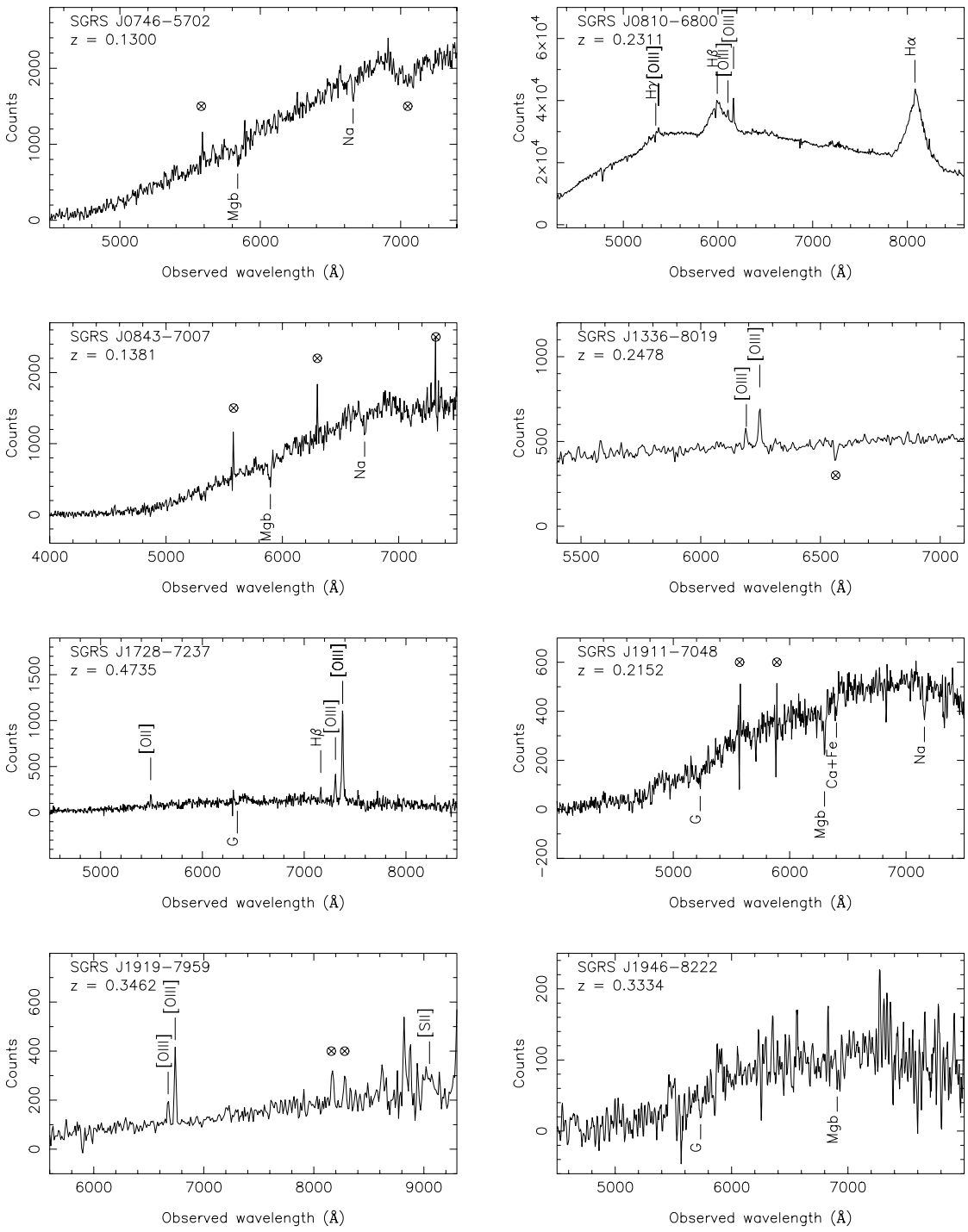

FIG. 19.—*Continued*

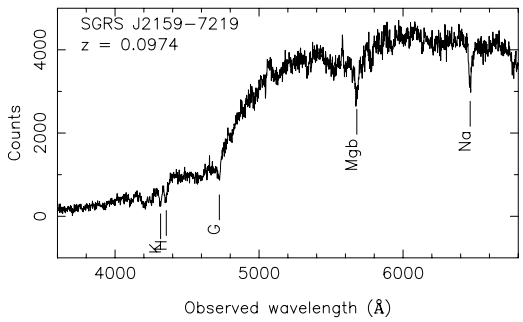

FIG. 19.—*Continued*

TABLE 7
REDSHIFTS AND SPECTRAL LINES

Name	Redshift	Prominent Lines
SGRS J0047−8307.....	0.2591 ± 0.0002	Absorption lines: Fe I λ4384, Hβ, and Mg *b*
SGRS J0143−5431.....	0.1791 ± 0.0001	Weak emission line: [O II] λ3727
		Absorption lines: K, H, G, Hβ, and Mg *b*
SGRS J0237−6429.....	0.364:	Weak emission lines: [O III] λλ4959, 5007
		Possible absorption line: Hβ
SGRS J0326−7730.....	0.2771 ± 0.0002	Moderate strength emission lines: [O III] λλ4959, 5007
		Absorption lines: K + H
SGRS J0331−7710.....	0.1456 ± 0.0001	Absorption lines: Mg *b* and Na
SGRS J0400−8456.....	0.1037 ± 0.0003	Absorption lines: Mg *b*, Ca + Fe, and Na
SGRS J0515−8100.....	0.1050 ± 0.0002	Weak emission lines: Hα, [N II] λ6583, and [S II] λλ6716, 6731
		Absorption lines: Mg *b*, Fe I, and Na
SGRS J0631−5405.....	0.2036 ± 0.0001	Quasar. Broad emission lines: Hβ and Hα
		Narrow emission lines: [O III] λλ4959, 5007
SGRS J0746−5702.....	0.1300 ± 0.0005	Absorption lines: Mg *b* and Na
SGRS J0810−6800.....	0.2311 ± 0.0002	Quasar. Broad emission lines: Hγ, Hβ, and Hα
		Narrow emission lines: [O III] λ4363, [O III] λλ4959, 5007
SGRS J0843−7007.....	0.1381 ± 0.0003	Absorption lines: Mg *b* and Na
SGRS J1336−8019.....	0.2478 ± 0.0001	Weak emission lines: [O III] λλ4959, 5007
SGRS J1728−7237.....	0.4735 ± 0.0002	Strong narrow emission lines: [O III] λλ4959, 5007
		Weak emission lines: [O II] λ3727, Hβ
		Absorption line: G
SGRS J1911−7048.....	0.2152 ± 0.0001	Absorption lines: Hδ, G, Mg *b*, Ca + Fe, and Na
SGRS J1919−7959.....	0.3462 ± 0.0002	Narrow emission lines: [O III] λλ4959, 5007 and possible [S II] λλ6716, 6731
SGRS J1946−8222.....	0.333:	Absorption lines: G and Mg *b*
SGRS J2159−7219.....	0.0974 ± 0.0001	Absorption lines: K, H, G, Mg *b*, and Na

NOTE.—Colons denote uncertain values.

TABLE 8
DERIVED PROPERTIES OF THE SUMSS GIANT RADIO SOURCES

Name	Redshift	Linear Size (Mpc)	1.4 GHz Core Power (10^{24} W Hz^{-1})	843 MHz Total Power (10^{26} W Hz^{-1})	M_b
SGRS J0047−8307.....	0.2591	1.34	1.7	1.1	−20.3
SGRS J0143−5431.....	0.1791	0.99	0.15	0.19	−20.6
SGRS J0237−6429.....	0.364:	2.24	0.9	0.64	−20.5
SGRS J0326−7730.....	0.2771	1.68	0.11[a]	0.84	−20.0
SGRS J0331−7710.....	0.1456	2.67	0.07	0.38	−21.0
SGRS J0400−8456.....	0.1037	0.71	0.08	0.05	−21.5
SGRS J0515−8100.....	0.1050	0.86	0.08	0.07	−21.1
SGRS J0631−5405.....	0.2036	1.03	4.4	0.81	−23.1
SGRS J0746−5702.....	0.1300	0.76	1.6	0.08	−20.9
SGRS J0810−6800.....	0.2311	1.28	0.05[a]	0.42	−23.9
SGRS J0843−7007.....	0.1381	0.81	0.6	0.10	−21.3
SGRS J1259−7737.....	>0.3	>1.5	>0.09	>1.25	<−18.5[b]
SGRS J1336−8019.....	0.2478	2.34	1.57	0.88	−23.7:[c]
SGRS J1728−7237.....	0.4735	2.2	9.95	1.79	−21.1[d]
SGRS J1911−7048.....	0.2152	1.24	0.16	0.32	−20.7
SGRS J1919−7959.....	0.3462	1.75	1.03	5.00	−19.3[e]
SGRS J1946−8222.....	0.333:	2.14	0.76	0.80	−18.9[e]
SGRS J2159−7219.....	0.0974	0.98	0.22	0.03	−21.6

NOTE.—Colons denote uncertain values.

[a] The core luminosity given for SGRS J0326−7730 and SGRS J0810−6800 is obtained using a 4.8 GHz core flux and assuming a flat core spectral index.

[b] The redshift lower limit is based on $K = 16.2 \pm 0.2$ mag, using the K-z relation for radio galaxies. The core luminosity is obtained using a 4.8 GHz core flux and assuming a flat core spectral index. The host galaxy is obscured; this is reflected in its absolute magnitude.

[c] The host galaxy is in a close pair in which the objects appear equally bright; the object to the north is a star. The galaxy magnitude, taken from Table 3, has been estimated by dividing the integrated magnitude equally between the two objects.

[d] The host galaxy of SGRS J1728−7237 is partly obscured by a star. The absolute magnitude is based on apparent magnitude judged from the neighborhood galaxies within 5″. The galaxy is likely to be more luminous.

[e] The host galaxies for SGRS J1919−7959 and J1946−8222 are obscured. This is reflected in their absolute magnitudes.

in surface brightness away from the center. This source appears to have a pair of jets close to the center and might be a giant edge-darkened radio source. The source has among the lowest radio powers in the sample, and this is consistent with the FR I–type structure.

The SUMSS is a survey with high surface brightness sensitivity; nevertheless, a large fraction (11/18) of the giant radio sources in the sample are observed to have emission gaps between the lobes. Continuous bridges are observed in SGRS J0400−8456, J0746−5702, J0843−7007, J1259−7737, J1336−8019, J1911−7048, and J1919−7959.

There are two quasars in the sample. Both the quasars (SGRS J0631−5405 and SGRS J0810−6800) have prominent lobes and have significantly more compact emission detected at the end of one of their lobes. While J0631−5405 has a bright radio core consistent with it being a quasar, the core in J0810−6800 is relatively weak. In both quasars the brighter lobe is observed to be closer to the core and is also the one containing the hot spot. No jets are seen in the ATCA images associated with the cores in these sources. Compared to the sources in the sample with classic FR II structure that have hot spots at one or both ends of the lobes, the two quasars have wider lobes with significantly lower axial ratio. It may be noted here that if the quasars are significantly foreshortened owing to projection, their linear sizes might be significantly larger than the estimates given in Table 8, and therefore, these quasars could potentially be the sources with the largest linear size in the sample. The giant quasars have intermediate radio powers compared to other giant radio sources in our sample.

The quasar fraction that we detect (two quasars in the sample of 18 giant radio sources) is smaller than that expected on the basis of the unification model for radio galaxies and quasars (Barthel 1989). This might be because giant radio sources with larger linear sizes are relatively rarer and our lower limit of 5′ to the angular size of sources accepted into the sample might imply a larger linear size cutoff for quasars as compared to radio galaxies.

Seven of the host galaxies of the giant radio sources in the sample have detections of narrow emission lines. Of these, SGRS J0326−7730, J1728−7237, and J1919−7959 have relatively stronger emission lines, whereas the emission lines in SGRS J0047−8307, J0237−6429, J0515−8100, and J1336−8019 are weaker. The giant radio sources in the sample with relatively higher redshifts and radio powers appear to be those with emission lines in their host spectra.

Asymmetry in lobe extents appears to be a characteristic of the sample. We define an asymmetry parameter as the ratio of the separation from the core of the farther lobe to the separation from the core of the closer lobe; distances to both lobes are measured to their farthest emission peaks. If we exclude the two quasars that might be affected by projection because their axes are likely to be at relatively smaller angles to the line of sight, 11 of the 16 giant radio sources have asymmetry parameter $\gtrsim$1.25: nearly 70% of the sample have radio lobes that are longer on one side by $\gtrsim$25%. Among the most asymmetric is SGRS J0331−7710, in which the southern lobe extends to $\gtrsim$2.5 times the distance of the northern lobe from the core.

Of the 11 asymmetric giant radio sources, the closer lobe is also the brighter of the two lobes in as many as 10 cases. This statistically significant result, which was earlier noted by Saripalli et al. (1986) for a small set of giant radio sources, has also been seen in other samples of giant radio sources (Schoenmakers et al. 2000b; Lara et al. 2001; Machalski et al. 2001). We do not, however, find a correlation between the lobe separation asymmetry and the lobe brightness asymmetry; although SGRS J0331−7710

is the most asymmetric in lobe separation and has lobes that are also very asymmetric in brightness, it is not among the most asymmetric in lobe brightness in the sample.

We define the misalignment angle as the supplement of the angle subtended by the two outermost hot spots at the core. Excluding the two quasars, the bent FR I SGRS J0400−8456, and the sources that have lobes with small axial ratio and no compact structure (SGRS J0143−5431, J0515−8100, J0746−5702, and J0843−7007), the distribution of misalignment angles shows that all the remaining 11 sources are aligned to within 10° on megaparsec scales; 7 of the 11 are aligned to within 5°.

The median linear size of our SUMSS sample is 1.3 Mpc, and the median total power is 5×10^{25} W Hz^{-1}. The giant radio sources in the sample have luminosities spread over more than 2 orders of magnitude covering the range $10^{24} < P^{843}_{\rm total} < 5 \times 10^{26}$ W Hz^{-1}, straddling the FR I/FR II break. The SUMSS giant radio sources exhibit increasing core power with total power. The correlation coefficient between the logarithm of the core power at 1.4 GHz and the logarithm of the total power at 843 MHz is only 0.5 for our sample; however, the fit is consistent with that found by Giovannini et al. (2001) for B2 and 3CR (Third Cambridge Revised Catalog of Radio Sources) radio galaxies that cover a larger range in total luminosity but have smaller linear size. In spite of its relatively low total power, SGRS J0746− 5702, which has a prominent partial jet toward its southwestern lobe, has a core power that is well above this fit to the core power versus total power: this is consistent with the earlier hypothesis that SGRS J0746−5702 is a restarted source. The only giant radio source in the sample with strong, narrow emission lines (SGRS J1728−7237) also has the most powerful radio core. Surprisingly, the giant radio source in our sample with the lowest core power is a quasar (SGRS J0810−6800).

7. SUMMARY

We have presented a complete sample of 18 giant radio sources compiled from the SUMSS; the sample satisfies the selection criteria: Galactic latitude $|b| > 12.^{\circ}5$, declination $\delta < -50^{\circ}$, and angular size >5′. All the sources have projected linear size larger than 0.7 Mpc (assuming $H_0 = 71$ km s^{-1} Mpc^{-1}). Higher resolution ATCA radio observations at 1.4 GHz have been used to identify radio cores and hot spots and distinguish any unrelated radio sources in the original candidate list. This facilitated optical identification and subsequent optical spectroscopy using the DBS at the 2.3 m SSO telescope and resulted in near-complete redshift information for our sample. The redshift range of the sample is 0.09–0.48. The 18 giant radio sources have powers straddling the FR I/FR II break power.

The SUMSS giants have radio morphologies that are mostly edge-brightened, although several have lobes with no compact features in them. Asymmetric lobe separation from their cores is widely seen, and a significant correlation exists between lobe separation and lobe brightness: the closer lobe is nearly always the brighter.

We detect all giants with linear size larger than 0.7 Mpc in the nearby universe ($z \leq 0.13$). However, given the selection criteria, there is inherently a redshift-dependent linear size bias at higher redshifts. Within this survey area ($z \leq 0.13$), not one of the four giants we detect has edge-brightened structure with compact hot spots. All four giants have among the lowest powers in the sample, and three have lobes with relaxed morphologies. If the three with relaxed morphologies are relicts of FR II giants, this suggests that in the nearby universe there could be an overabundance of giant radio sources with relict lobes as compared to giants whose lobe ends are currently energized by beams.

The SUMSS sample has several interesting sources. The sample contains one of the most asymmetric giant radio sources, SGRS J0331−7710, where not only is one lobe about 2.5 times closer to the core than the opposite lobe, it is also more than 2.5 times brighter. The four giant radio sources SGRS J0143−5431, J0746−5702, J1946−8222, and J2159−7219, as well as SGRSC 0414−6933, are candidates for restarted activity: all have relaxed outer lobes and either a pair of inner lobes that might be a manifestation of new beams from the central engine or partial jets close to the center.

MOST is operated by the University of Sydney and supported in part by grants from the Australian Research Council. ATCA is part of the Australia Telescope, which is funded by the Commonwealth of Australia for operation as a National Facility managed by CSIRO. We acknowledge the use of SuperCOSMOS, an advanced photographic plate digitizing machine at the Royal Observatory of Edinburgh, in the use of digitized images for the radio-optical overlays. We thank Anton Koekemoer for discussions in the early part of the project and for advice on some IRAF tasks. We thank Helen Johnston for the *K*-band image of SGRS J1259−7737.

APPENDIX A

CANDIDATES NOT IN THE COMPLETE SAMPLE OF GIANT RADIO SOURCES

In Figures 20–28 we present 843 MHz SUMSS and higher resolution ATCA images of a selection of giant radio source candidates from the original list that did not satisfy one or both criteria, angular size >5′ or projected linear size larger than 0.7 Mpc. We obtained low-resolution optical spectra using the DBS on the 2.3 m SSO telescope for the host galaxies of some of these candidates, and Boyce (2000) obtained Anglo-Australian Telescope spectra for some hosts; the spectra are presented in Figure 29. Table A1 lists the prominent spectral lines and the derived redshifts. In Table A2 we give the sizes and structural type for some of these radio sources. In Table A3 we list their radio core positions and the 1.4 GHz core flux densities. For all the sources from the original giant radio source candidate list that were rejected from the final sample we give brief notes below.

A1. SGRSC J0020−7321 (FIG. 20)

The SUMSS image shows a filled radio structure over its 4.′8 extent. In the higher resolution 1.4 GHz ATCA image the eastern lobe is completely resolved (Fig. 20*a*). There is structure seen in the western lobe; however, no compact hot spot is observed. The 4.8 GHz ATCA image detects a core at the position of a bright galaxy (Fig. 20*b*). Twin jetlike structures are seen at the core and aligned with the source axis; the western jet appears to curve toward the bright elongated structure in the western lobe. The host has a close companion 4″ to the northwest, and there is a prominent halo surrounding the galaxy pair. This candidate is rejected because it fails the angular size criterion. The optical spectrum was obtained by Boyce (2000).

A2. SGRSC J0129−6433 (FIG. 21)

The SUMSS image shows a filled radio structure with a straight edge along its southwestern boundary. The radio structure is

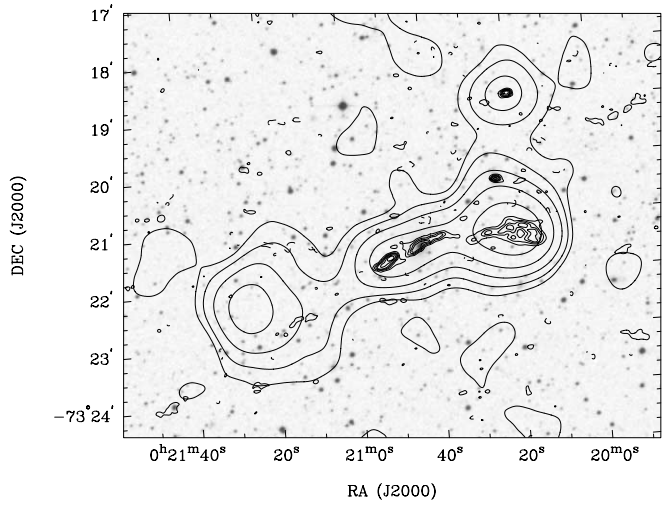

FIG. 20*a*

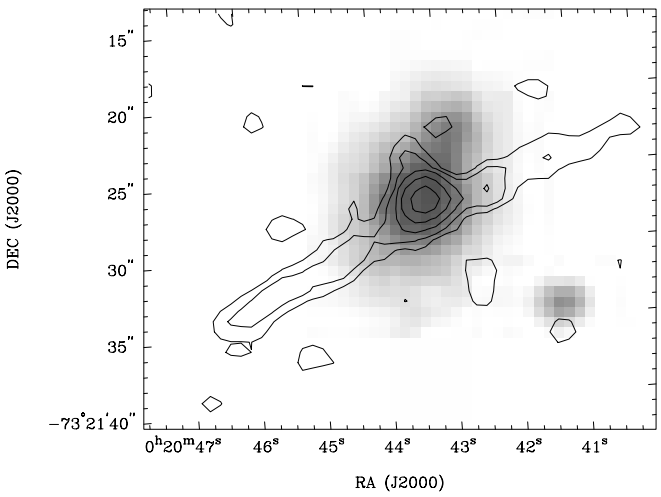

FIG. 20*b*

FIG. 20.—SGRSC J0020−7321 radio contours on the red SSS optical gray-scale image. An ATCA 4.8 GHz image of the core is shown in (*b*). SUMSS contours (*thick lines*) are at −1, 1, 2, 4, 8, and 16 × 3 mJy beam^{-1}, and ATCA contours (*thin lines*) are at −1, 1, 2, 3, 4, 6, and 8 × 0.5 mJy beam^{-1} (1.4 GHz) and at −1, 1, 2, 3, 4, and 6 × 0.1 mJy beam^{-1} (4.8 GHz). The beams have FWHMs of 47.″3 × 45″ (SUMSS), 7.″3 × 5.″2 (ATCA, 1.4 GHz), and 2.″1 × 1.″9 (ATCA, 4.8 GHz).

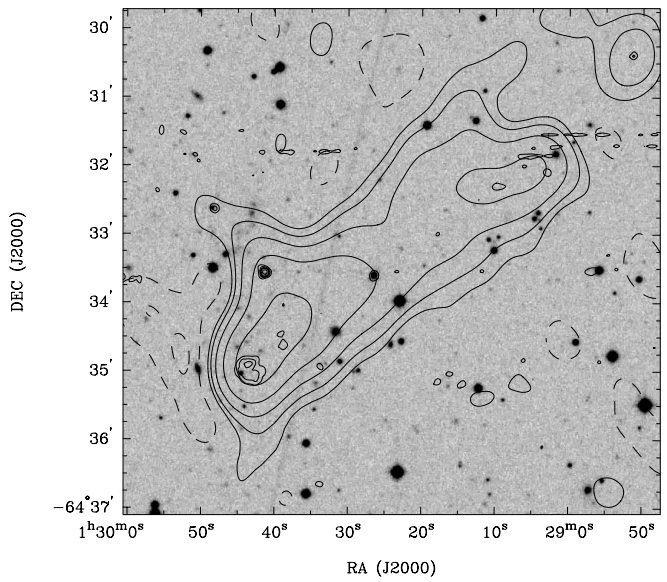

FIG. 21.—SGRSC J0129−6433 radio contours on the blue SSS optical gray-scale image. SUMSS contours (*thick lines*) are at −1, 1, 2, 4, 8, and 16 × 3 mJy beam^{-1}, and ATCA contours (*thin lines*) are at 1, 2, 3, 4, and 6 × 0.8 mJy beam^{-1}. The beams have FWHMs of 50.″1 × 45″ (SUMSS) and 6.″5 × 5.″8 (ATCA).

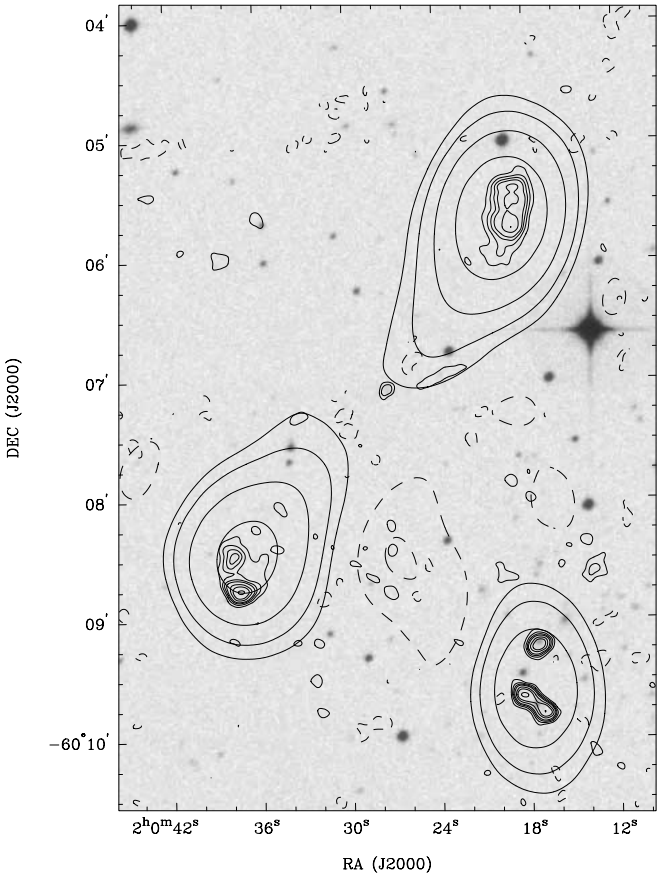

FIG. 22.—SGRSC J0200−6007 radio contours on the blue SSS optical gray-scale image. SUMSS contours (*thick lines*) are at −1, 1, 2, 4, and 8 × 5 mJy beam^{-1}, and ATCA contours (*thin lines*) are at −1, 1, 2, 3, 4, 6, 8, and 12 × 0.5 mJy beam^{-1}. The beams have FWHMs of 52″ × 45″ (SUMSS) and 6.″6 × 5.″9 (ATCA).

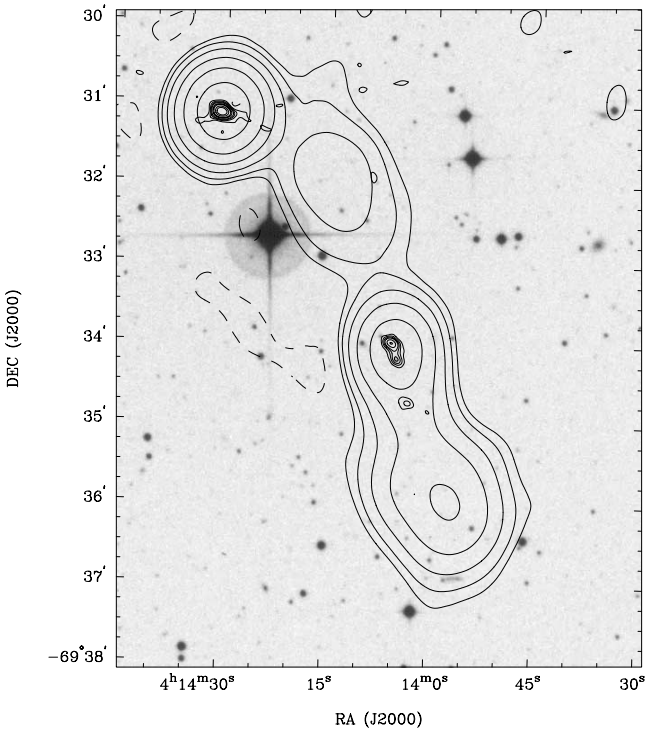

FIG. 23*a*

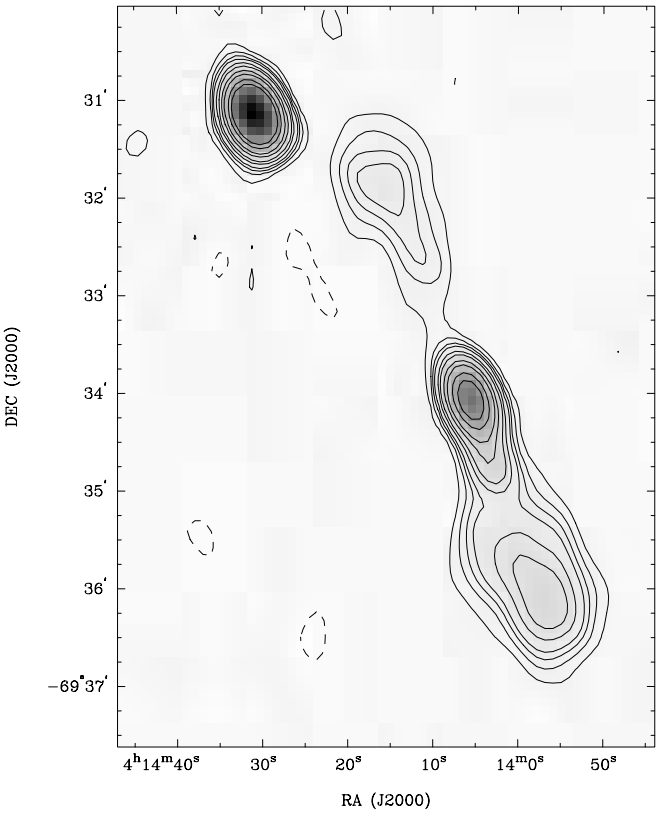

FIG. 23*b*

FIG. 23.—SGRSC J0414−6933 radio contours on the blue SSS optical gray-scale image. SUMSS contours (*thick lines*) are at −1, 1, 2, 4, 8, 16, and 32 × 3 mJy beam^{-1}, and ATCA contours (*thin lines*) are at (*a*) −1, 1, 2, 3, 4, 6, 8, 12, and 16 × 3 mJy beam^{-1} and (*b*) −2, −1, 1, 2, 3, 4, 6, 8, 12, 16, 24, and 32 × 1.2 mJy beam^{-1}. The beams have FWHMs of 48″.5 × 45″ for SUMSS and (*a*) 9″ × 6″.2 and (*b*) 32″.7 × 21″.5 for ATCA.

reminiscent of the structure seen in 3C 430 and 3C 111, where one edge of the radio galaxy has a straight edge and lobe emission on the opposite side extends away perpendicular to the radio axis. The ATCA image shows a compact feature that appears to be a multiple hot spot structure at the end of the southeastern lobe; the northern lobe is resolved. There are two presumably unrelated sources seen in the ATCA image within the southern lobe. The host galaxy of this source has strong narrow emission lines and is fairly isolated. The closest neighbors are about 1′ away to the southeast and southwest. The candidate fails the angular size criterion and is excluded from our sample.

A3. SGRSC J0152−8020

In the SUMSS image (not shown) the source is seen as two extended components separated by about 5′.5. Both components of this candidate are detected in the higher resolution ATCA observations in which the southwestern source is identified with a faint optical object and the northeastern source has a double structure at a position angle of −20°. The candidate is rejected because the western component is identified and both SUMSS components are likely to be separate sources.

A4. SGRSC J0200−6007 (FIG. 22)

Two prominent lobes are observed in the SUMSS image. The ATCA observations detect structure in both lobes; also, a compact core is detected between the two components. The core is identified with a faint $b_J = 21.2$ galaxy; we have not obtained an optical spectrum for the host galaxy. This candidate is rejected because its angular extent is less than 5′.

A5. SGRSC J0414−6933 (FIG. 23)

Four extended components are seen in the SUMSS image of this candidate. The higher resolution ATCA image shows a compact source coincident with the northernmost component. The other three SUMSS components are observed to constitute a separate triple radio source in the low-resolution ATCA image (Fig. 23*b*): the central component of this triple is resolved into a 45″ triple in the higher resolution ATCA image (Fig. 23*a*), and the core is identified with a $b_J = 19.5$ galaxy. The lack of compact features in the two lobes and the central triple structure suggest restarting activity in this radio galaxy. The optical host has a halo that is more prominent in the red and has a sharp edge toward the southwest. It has no immediate neighbors, although it might be a member of a loose group. The 4′.5 triple radio source is a giant radio source; however, J0414−6933 is not part of the sample because its angular size is less than 5′. The optical spectrum for this source (Fig. 29) was obtained using the DBS at the 2.3 m telescope at SSO. The spectrum was obtained from a single 2000 s exposure on 2002 November 4.

A6. SGRSC J0534−8203

This source is observed to be two separate components in the SUMSS image (not shown); the candidate has a total angular size of less than 5′ and therefore fails the selection criterion. In the ATCA image (not shown) the eastern component is resolved into a 1′ triple; there is a faint blue galaxy very close to the central component of this triple, which is likely to be the host galaxy for the eastern SUMSS component. The western component is

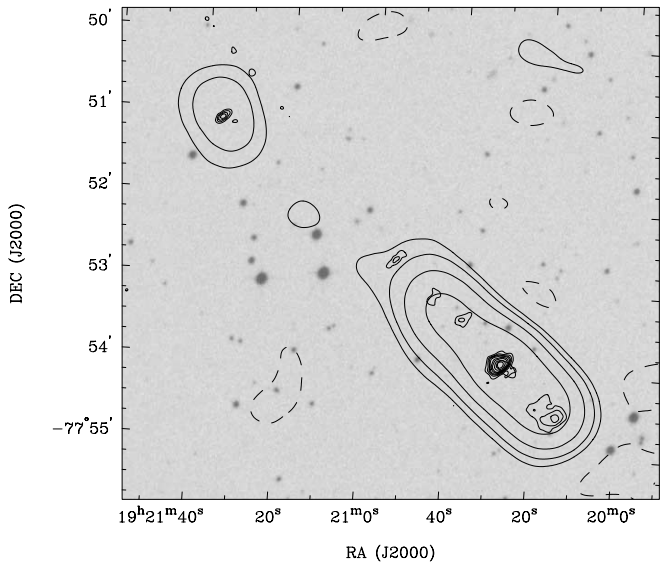

FIG. 24*a*

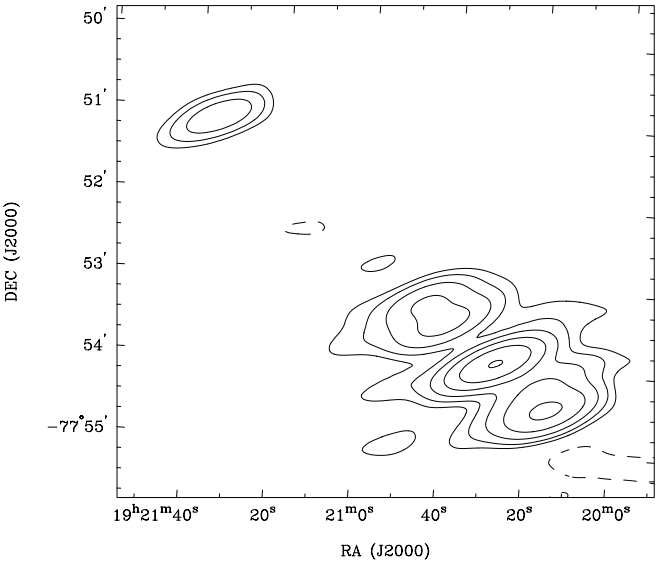

FIG. 24*b*

FIG. 24.—SGRSC J1920−7753 radio contours on the red SSS optical gray-scale image. SUMSS contours (*thick lines*) are at −1, 1, 2, 4, 8, and 16 × 3 mJy beam^{-1}, and ATCA contours (*thin lines*) are at −1, 1, 2, 3, 4, 6, 8, 12, and 16 × 0.8 mJy beam^{-1}. The beams have FWHMs of 46.″4 × 45″ (SUMSS) and 10.″3 × 4.″3 (ATCA). A 1.4 GHz ATCA image with a resolution of 52.″2 × 19″ is shown in (*b*); contour levels are at −1, 1, 2, 3, 4, 6, and 8 × 0.8 mJy beam^{-1}.

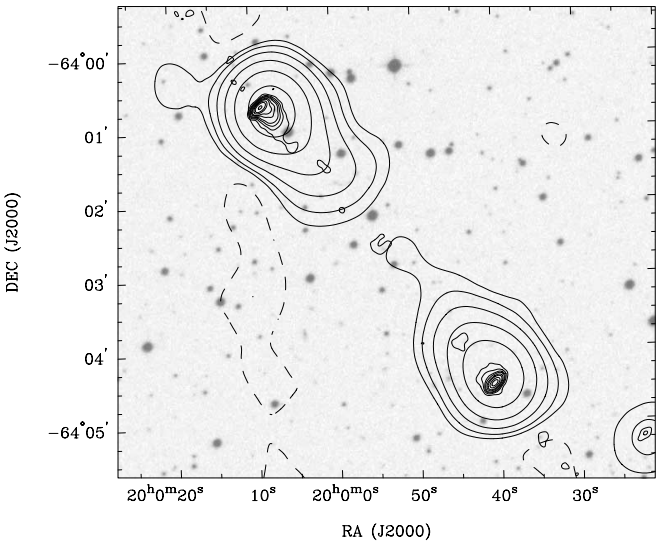

FIG. 25.—SGRSC J1959−6402 radio contours on the red SSS optical gray-scale image. SUMSS contours (*thick lines*) are at −1, 1, 2, 4, 8, 16, and 32 × 5 mJy beam^{-1}, and ATCA contours (*thin lines*) are at −1, 1, 2, 3, 4, 6, 8, 12, 16, and 24 × 3 mJy beam^{-1}. The beams have FWHMs of 50.″1 × 45″ (SUMSS) and 12.″2 × 5.″4 (ATCA).

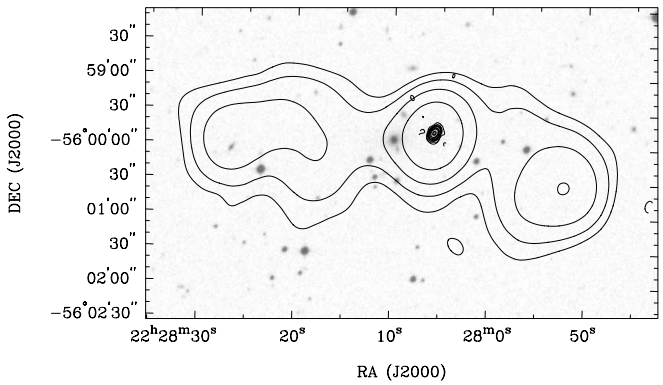

FIG. 26.—SGRSC J2228−5600 radio contours on the blue SSS optical gray-scale image. SUMSS contours (*thick lines*) are at −1, 1, 2, 4, 8, and 16 × 3 mJy beam^{-1}, and ATCA contours (*thin lines*) are at −1, 1, 2, 3, 4, 6, 8, and 12 × 3 mJy beam^{-1}. The beams used have FWHMs of 54.″3 × 45″ (SUMSS) and 9.″3 × 6.″6 (ATCA).

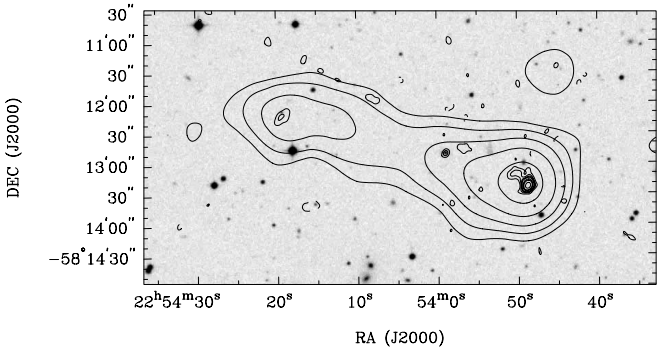

FIG. 27.—SGRSC J2253−5813 radio contours on the blue SSS optical gray-scale image. SUMSS contours (*thick lines*) are at −1, 1, 2, 4, 8, and 16 × 4 mJy beam^{-1}, and ATCA contours (*thin lines*) are at −1, 1, 2, 3, 4, 6, 8, and 12 × 2 mJy beam^{-1}. The beams have FWHMs of 52″ × 45″ (SUMSS) and 8.″9 × 6.″6 (ATCA).

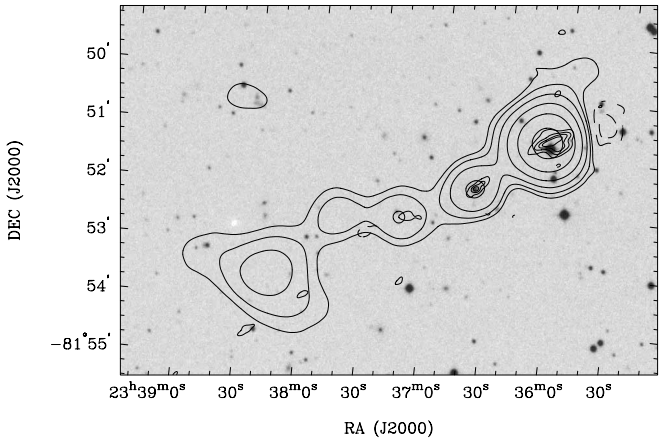

FIG. 28.—SGRSC J2336−8151 radio contours on the blue SSS optical gray-scale image. SUMSS contours (*thick lines*) are at −2, −1, 1, 2, 4, 8, 16, and 32 × 4 mJy beam^{-1}, and ATCA contours (*thin lines*) are at −1, 1, 2, 3, and 4 × 2.5 mJy beam^{-1}. The beams have FWHMs of 45.″7 × 45″ (SUMSS) and 8.″8 × 5.″9 (ATCA).

resolved into three compact sources, none of which has an optical counterpart in SSS.

A7. SGRSC J0551−5655

This source consists of three extended components in the SUMSS image (not shown). Higher resolution ATCA observations show the western component to be a double centered on an optical galaxy; in addition, compact components without optical counterparts in SSS images are detected coincident with the other two SUMSS components. The candidate has an angular size of less than 5′ and hence fails the selection criteria.

A8. SGRSC J0603−5429

In the SUMSS image (not shown) the source is seen as three peaks that are connected by extended emission. In the higher resolution 1.4 GHz ATCA observations, the southeastern peak appears as an unresolved component without any optical counterpart in the SSS images. The remaining two peaks are also detected: they are weaker and appear to be coincident with two faint galaxies. This source is rejected as a candidate because its peak-to-peak angular size is less than 5′.

A9. SGRSC J0622−5938

In the SUMSS image (not shown) the source appears as two components that are extended roughly toward each other with a faint bridge of emission connecting them. ATCA detects weak components at the two peaks, and these have no optical counterparts in the SSS images. The candidate has an angular size of less than 5′ and fails the selection criteria.

A10. SGRSC J0745−7732

In both the SUMSS and the ATCA images (not shown), this source is observed to be a chain of nine unresolved radio sources arrayed along a position angle of about 45°. Some of the components are extended along this position angle in the SUMSS; however, there is no diffuse emission connecting these individual sources. Only two components have faint objects associated with them in the blue SSS image. Apart from being in a line, there is no evidence from either the SUMSS or ATCA observations that the remaining components form a single source, and therefore, we do not accept this into our giant radio source sample.

A11. SGRSC J1920−7753 (FIG. 24)

The SUMSS image shows a very elongated radio structure directed toward a component to the northeast (Fig. 24*a*). Low-resolution 20 cm ATCA imaging reveals that the elongated source is a triple (Fig. 24*b*). In the higher resolution ATCA image the elongated source is resolved into a series of peaks, and the brightest (with flux density 19.4 mJy beam^{-1}) is identified with a very faint object that is seen only in the red SSS image. The northeastern component is detected as an unresolved source without any optical identification in SSS. Because the SUMSS components are deemed to be separate sources that are <5′ in size, the source is excluded from the sample.

A12. SGRSC J1959−6402 (FIG. 25)

The SUMSS image shows this source to be two edge-brightened lobes; ATCA images show compact hot spots at the leading edges. A weak core is detected with a flux density of 4.3 mJy beam^{-1} at 1.4 GHz. The angular size as measured between the hot spots detected in the ATCA image is just under 5′, and the source fails the selection criteria for our sample.

A13. SGRSC J2150−6210

In the SUMSS image (not shown) the source has a double structure, with significantly different flux densities, and a connecting bridge. ATCA detects a compact source at the location of the stronger northeastern component and a weaker source at the peak of the southwestern SUMSS component. The northeastern source is identified with a bright elliptical galaxy and is likely to be a separate source. The candidate is rejected, as it fails the angular size criterion.

A14. SGRSC J2222−5617

Two separate components appear in the SUMSS image (not shown), and the southern component has a weak extension toward the other component. The ATCA observations reveal the two components to be a double and a triple, respectively. The southern triple is identified in SSS with an elliptical galaxy. The two SUMSS components are likely to be two unrelated radio sources.

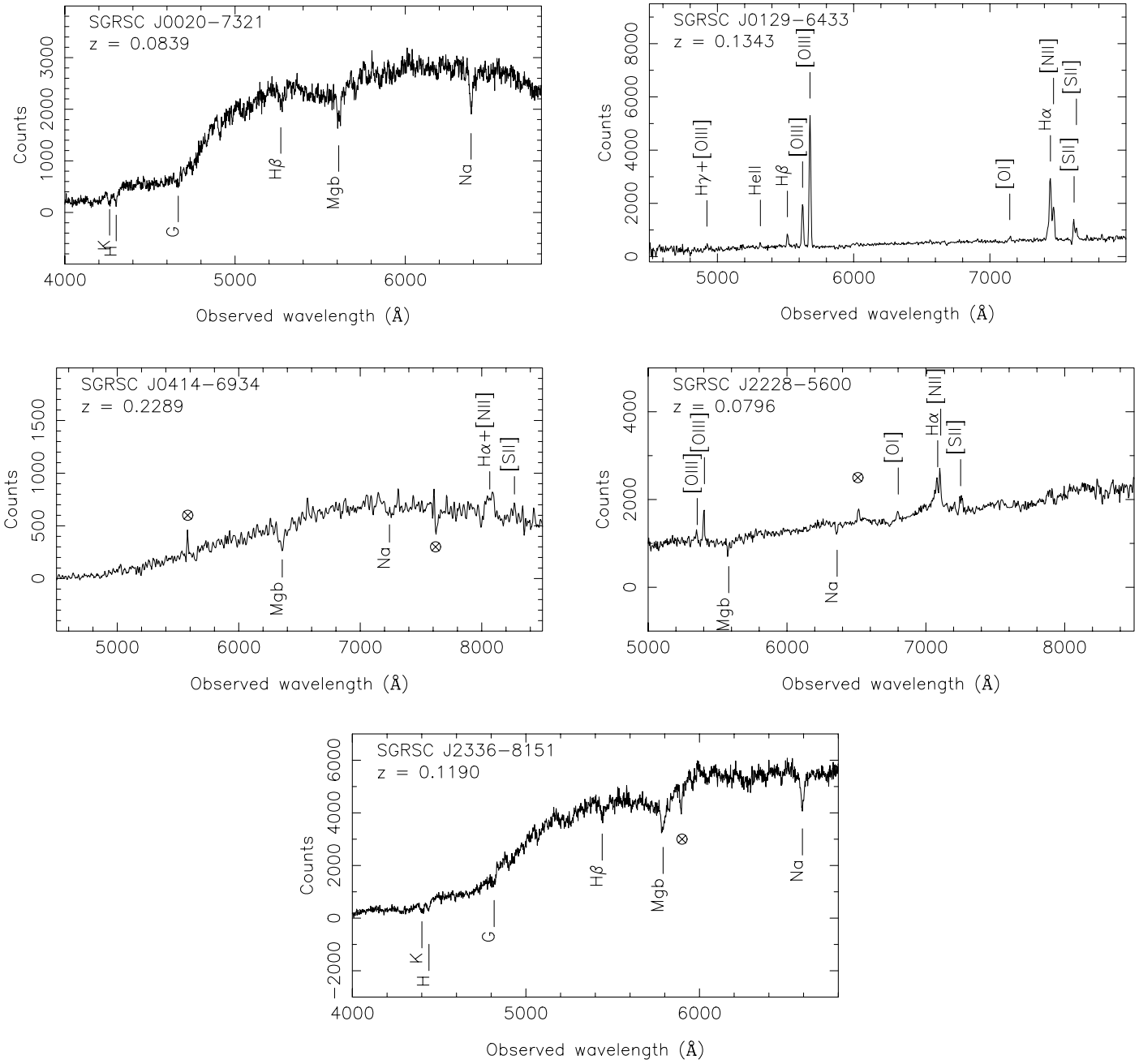

FIG. 29.—Optical spectra of the candidates that are not in the complete sample of giant radio sources.

TABLE A1

REDSHIFTS AND SPECTRAL LINES IN SPECTRA IN FIGURE 29

Name	Redshift	Prominent Lines
SGRSC J0020−7321.....	0.0839 ± 0.0001	Absorption lines: K, H, G, Hβ, Mg *b*, and Na
SGRSC J0129−6433.....	0.1343 ± 0.0002	Strong narrow emission lines: Hβ and [O III] $\lambda\lambda$4959, 5007, Hα + [N II] blend and [S II] $\lambda\lambda$6716, 6731 Weak emission lines: Hγ + [O III] λ4363, He II λ4686, and [O I] λ6300
SGRSC J0414−6933.....	0.228:	Possible weak emission lines: Hα + [N II] blend and [S II] $\lambda\lambda$6716, 6731 Absorption lines: Mg *b* and Na
SGRSC J2228−5600.....	0.0796 ± 0.0002	Strong emission lines: [O III] $\lambda\lambda$4959, 5007, [O I] λ6300, Hα + [N II] blend, and [S II] $\lambda\lambda$6716, 6731 Absorption lines: Mg *b* and Na
SGRSC J2336−8151.....	0.1190 ± 0.0001	Absorption lines: K, H, G, Hβ, Mg *b*, and Na

NOTE.—Colons denote uncertain values.

TABLE A2

PARAMETERS FOR SOME OF THE REJECTED CANDIDATES

Name	Other Names	SUMSS Components	Redshift	Angular Size (arcmin)	Type FR I/FR II	Linear Size (Mpc)
SGRSC J0020−7321	PMN J0020−7321	J002046−732132	0.0839	4.8	FR II	0.45
	PMN J0021−7322	J002021−732115				
		J002124−732219				
SGRSC J0129−6433	PMN J0129−6433	J012934−643353	0.1343	4.7	FR II	0.66
		J012913−643223				
		J012941−643447				
SGRSC J0200−6007	PMN J0200−6007	J020019−600541	...	4.2	FR II	...
		J020036−600825				
SGRSC J0414−6933	PMN J0414−6933	J041404−693407	0.228:	4.5	FR II	0.98
		J041358−693552				
		J041414−693159				
SGRSC J1959−6402	PKS B1955−641	J195941−640420	...	4.9	FR II	...
	PMN J1959−6403	J200007−640044				
	PMN J2000−6400					
SGRSC J2228−5600	PMN J2228−5559	J222753−560030	0.0796	4.8	FR II	0.43
		J222823−555953				
		J222805−555950				
SGRSC J2253−5813	PMN J2253−5812	J225350−581319	...	4.3	FR II	...
		J225411−581225				
SGRSC J2336−8151	PMN J2336−8151	J233607−815045	0.1190	5.4	FR II	0.68
		J233816−815332				
		J233639−815139				

NOTE.—Colons denote uncertain values.

TABLE A3

RESULTS OF ATCA OBSERVATIONS OF THE SOURCES IN TABLE A2

	CORE POSITIONS (J2000.0)		CORE FLUX DENSITY (mJy)	
NAME	R.A.	Decl.	1.4 GHz	4.8 GHz
SGRSC J0020−7321	00 20 43.3	−73 21 26.9	...	2.5
SGRSC J0129−6433	01 29 26.5	−64 33 36.0	3.9	
SGRSC J0200−6007	02 00 27.4	−60 07 04.9	2.3	
SGRSC J0414−6933	04 14 05.0	−69 34 11.5	12.9	
SGRSC J1959−6402	19 59 53.9	−64 02 36.1	4.3	
SGRSC J2228−5600	22 28 05.7	−55 59 48.2	40.2	
SGRSC J2253−5813	22 53 59.0	−58 12 49.8	5.4	
SGRSC J2336−8151	23 36 39.6	−81 51 41.2	9.4	

NOTE.—Units of right ascension are hours, minutes, and seconds, and units of declination are degrees, arcminutes, and arcseconds.

A15. SGRSC J2228−5600 (FIG. 26)

The SUMSS image shows this source to be an edge-brightened radio source with a relatively strong core. The 1.4 GHz ATCA image shows only the core component as a strong unresolved source coincident with a relatively bright $b_J = 17.7$ elliptical galaxy. The host is likely to be in a cluster. The galaxy optical spectrum shows the presence of moderately strong emission lines. This source has a linear size of 428 kpc and is not a giant radio source.

A16. SGRSC J2253−5813 (FIG. 27)

The SUMSS image shows an edge-brightened double radio source with a continuous bridge. Higher resolution ATCA observations detect hot spot components at both ends, as well as a radio core that is identified with a $b_J = 18.5$ elliptical galaxy. We have not obtained an optical spectrum for this galaxy. This source is not in the sample because its angular size $<5'$.

A17. SGRSC J2336−8151 (FIG. 28)

The SUMSS image shows a chain of connected components. Our higher resolution ATCA image shows emission features associated with all components except the diffuse component at the southeastern end of the source. A radio core, coincident with an optical counterpart, is detected in an inner component, and there is an indication of a twin-jet structure close to the core. The radio structure is very asymmetric. This source fails the linear size criterion and hence is not part of our giant radio source sample. The optical spectrum was obtained by Boyce (2000).

REFERENCES

Barthel, P. D. 1989, ApJ, 336, 606
Becker, R. H., White, R. L., & Helfand, D. J. 1995, ApJ, 450, 559
Bock, D. C.-J., Large, M. I., & Sadler, E. M. 1999, AJ, 117, 1578
Boyce, E. 2000, honors thesis, Univ. Sydney, http://www.astrop.physics.usyd.edu.au/SUMSS/PAPERS/boyce_honours.pdf
Condon, J. J., Cotton, W. D., Greisen, E. W., Yin, Q. F., Perley, R. A., Taylor, G. B., & Broderick, J. J. 1998, AJ, 115, 1693
Cotter, G., Rawlings, S., & Saunders, R. 1996, MNRAS, 281, 1081
Giovannini, G., Cotton, W. D., Feretti, L., Lara, L., & Venturi, T. 2001, ApJ, 552, 508
Lara, L., Cotton, W. D., Feretti, L., Giovannini, G., Marcaide, J. M., Marquez, I., & Venturi, T. 2001, A&A, 370, 409
Machalski, J., Jamrozy, M., & Zola, S. 2001, A&A, 371, 445
Mauch, T., Murphy, T., Buttery, H. J., Curran, J., Hunstead, R. W., Piestrzynski, B., Robertson, J. G., & Sadler, E. M. 2003, MNRAS, 342, 1117
Owen, F. N., & Ledlow, M. J. 1994, in ASP Conf. Ser. 54, The First Stromlo Symposium: The Physics of Active Galaxies, ed. G. V. Bicknell, M. A. Dopita, & P. J. Quinn (San Francisco: ASP), 319
Padovani, P., & Urry, C. M. 1992, ApJ, 387, 449
Perlman, E. S., Padovani, P., Giommi, P., Sambruna, R., Jones, L. R., Tzioumis, A., & Reynolds, J. 1998, AJ, 115, 1253
Rengelink, R. B., Tang, Y., de Bruyn, A. G., Miley, G. K., Bremer, M. N., Roettgering, H. J. A., & Bremer, M. A. R. 1997, A&AS, 124, 259
Rodgers, A. W., Conroy, P., & Bloxham, G. 1988, PASP, 100, 626
Saripalli, L., Gopal-Krishna, Reich, W., & Kuehr, H. 1986, A&A, 170, 20
Saripalli, L., Subrahmanyan, R., & Udaya Shankar, N. 2002, ApJ, 565, 256
———. 2003, ApJ, 590, 181
Schoenmakers, A. P., de Bruyn, A. G., Roettgering, H. J. A., & van der Laan, H. 2001, A&A, 374, 861
Schoenmakers, A. P., de Bruyn, A. G., Roettgering, H. J. A., van der Laan, H., & Kaiser, C. R. 2000a, MNRAS, 315, 371
Schoenmakers, A. P., Mack, K.-H., de Bruyn, A. G., Roettgering, H. J. A., Klein, U., & van der Laan, H. 2000b, A&AS, 146, 293
Subrahmanyan, R., & Saripalli, L. 1993, MNRAS, 260, 908
Subrahmanyan, R., Saripalli, L., & Hunstead, R. W. 1996, MNRAS, 279, 257